Universiteit Leiden

Master Computer Science

Topology by pressure in plant tissue: A study on virtualleaf, waterflux and division methods.

Name:	W.R.D. Venemans
Student ID:	s2325217
Date:	August 24, 2025
Specialisation:	Bioinformatics
1st supervisor:	R.M.H. Merks
2nd supervisor:	L. Cao

Master's Thesis in Computer Science

Leiden Institute of Advanced Computer Science (LIACS)
Leiden University
Niels Bohrweg 1
2333 CA Leiden
The Netherlands

Abstract

Growing is one of the most important processes within a plant. In plant tissue, plant cells grow, shrink and divide and are tightly packed together. The topology of these cells is widely studied and is important to the stability of the tissue. Another stability-enforcing factor is the turgor pressure in the cells, which is the force that the cell interior components put on the cell wall and, as such, puts constraint on the tissue. In this paper, the model virtualleaf will be studied in the light of the turgor pressure and these topological properties. An extension to the model, to study the water uptake of each of the cells, which is the crucial factor for cell growth, is added, and the behaviour in a two-cell and a multicellular model cell is discussed. This paper shows that the virtualleaf simulations do not show the same topological properties compared to nature. Additionally, the expansion of the model with the waterflux does not change this perspective but does change intrinsic topological properties and gives rise to different behaviours in a two-cell and in a multicellular study. We showed that wall manipulation lead to growth inequalities, but only for a certain parameter sets. This thesis serves as a starting point to expand virtualleaf with the waterflux expansion and show the potential this model offers.

Contents

Acknowledgments

I want to dedicate this thesis to my dog Pien who passed away this year. I hope they have a lot of treats (and cheese) in dog heaven.

I want to thank Roeland for his help, inspiration and his never ending patience for my thesis!

This work was performed using the compute resources from the Academic Leiden Interdisciplinary Cluster Environment (ALICE) provided by Leiden University.

1 Introduction

Growth is one of the most essential processes in plants, ensuring the survival of the plant. Every part of the plant is made out of plant cells, which, in contrast to animal cells, are stuck in place and tightly packed. The growth process of tissue in plants is also different than in animal cells: each cell has a vacuole in which it stores water, which can take up or give off water to their surroundings, either to the neighbouring cells through their shared walls or the apoplast; In between the cell walls, there is a space where water flows freely and solutes can be exchanged, which is called the apoplast. The cell wall plays an essential role in the shape and the transport of water in the cell; it consists of two parts: the inside wall, which is a flexible wall surrounding the cell nucleus and organelles and the outer wall, which is a rigid wall mainly made out of cell fibres. These walls are permeable and can let water through; cells can take up water by waterfluxes caused by osmotic pressure differences between the cell, which is the difference in solute concentration between the exterior and the interior of the cell. As the water enters the cell, the cell volume increases, generating turgor pressure. This turgor pressure pushes the inside of the cell against the walls of the cell, causing the walls to stretch. This stretching is often modelled as an irreversible viscoplastic yielding mechanism in plant cells, where the cell walls can be stretched when the yielding threshold is reached, as defined by Lockhart's equation [1]. This stretching of the walls enables plant cells to keep their structural integrity while also still being able to stop growing [2] [3]. Contrary to animal cells, where cell size is one of the most important thresholds in signalling when to divide [4], plant cells are more complex. In earlier stages of leaf development, the size of the cell is the most important threshold. However, later on, the plant favours cell growth and signalling of other proteins as the signal for cell division [5] [6].

The aforementioned turgor pressure in the cell is a consequence of the water uptake of the cell and the following cell expansion that leads to the pressure on the cell walls by the cell content. The cell walls react to this pressure by yielding, which was first modelled by Lockhart in 1965 [1], proposing an irreversible or plastic cell wall expansion. This model was extended further in 1985 by Ortega, with the extension of elastic wall yielding [7]. But there are also many other challenges for the modelling of growth, such as the cell packaging [8] [9], gene regulation of growth [10], and the division methods inside a tissue [11]. All these different mechanisms make the already challenging process of modelling plant tissue difficult to represent, especially if the goal is to observe the growth and stabilisation of multicellular systems. To cut down on computer cost and complexity, simplifications to the models are made in a two-dimensional setting, such as the representation of cells as a vertex-based polygonal network in the two-dimensional space [12] or in the three-dimensional space [13].

The consequence of the turgor pressure and the cell divisions is that the cells within plant tissue have a variety of shapes and sizes, resulting in different geometries. Cell packaging is an inherent effect of the ability of cells to modulate their contact with other cells. It allows the cells to form different topologies and cover a diverse area. The first notion of the topology within plant tissue was done in 1928, where Lewis noted that the number of neighbours of cells within tissue was reproducible and averaged to a near-perfect 6 neighbours per cell [14]. This observation was expanded by Gibson et al., who argued through Euler's equations that in the hypothetical case of infinite tissues, the average amount of neighbours should be exactly 6. This was confirmed by the same study, which tried to explain the appearance of this 'perfect' number: the proliferation of cells alone drives the tissue towards this number, showing that the tissue is dominated by mostly hexagons, having six sides [9]. Another model by Farhadifar

et al. [8] showed that the packaging of cells can be more accurately predicted by the addition of physical properties of the cell, which included the area elasticity, line tension and perimeter contractility. This was also confirmed *in vitro*, where the model was able to replicate experimental data, including laser-ablated tissue [8].
Another observation was made by Lewis that the area of the cells is linearly related to the number of neighbours in the cell. He proposed the relation of the area of a n-sided cell A_n to be linearly dependent as $A_n = (n-2)a$, with a representing a constant, calculated by taking the average area of all the cells with six sides and dividing it by four. This observation was coined the 'Lewis law'. The Lewis law has been developed further by biologists and crystallographers alike, generalising the formula to a linear relation between the area and the number of neighbours [15]. The Lewis law was shown to hold when every cell within the tissue has at least three neighbours, which may not be the case in some tissues. To further articulate on this edge case, Rivier proposed a more robust formulation of the Lewis law using the maximum entropy method, but was later shown to be incompatible with verifying this law [15]. A possible mechanical explanation for the Lewis law has been proposed by Kokic et al., which showed that the Lewis law is a direct result of the energy minimisation of cells: while a tissue tries to minimise their surface energy, cells adhere to a regular polygonal shape, giving rise to a linear relation. When the area between the areas increases beyond atypical levels, the authors describe the Lewis law to be quadratic instead of linear [16].
The aforementioned study by Farhadifar et al. [8] and Gibson et al. [9] has shown the importance of cell proliferation within the topology and packing of the cells and thus the tissue. Cells proliferate by dividing themselves into two daughter cells; Cell division is a research field with a rich history, where there have been numerous division rules that explain the choice of division plane. It started with the observation of Hofmeister in 1863, where he noticed that cells divide over their perpendicular axis of cell expansion. Shortly thereafter, the most prominent rule was described by Errera, where he discovered a remarkable resemblance between cells and soap bubbles. In 1888, he discovered that the behaviour of soap bubbles mirrors that of plant cells: 'the cell plate, at the time of its formation, adopts the geometry that a soap film would take under the same conditions' [17] . This rule, named 'Errera's Rule', simplifies that cells choose to divide over their shortest axis to minimise the surface area and thus have two daughter cells of the same size[17]. For a long time, this rule was accepted to be true for all plant tissues. However, further research showed that cells do not always choose this shortest axis when dividing, which indicates that Errera's rule is not enough to model the complete division procedure. The main critique was that cells in tissue choose a different division axis based on their location in the plant tissue and do not universally choose the shortest axis[18]. An expansion on Errera's rule was proposed by Besson and Dumais, where the cell chooses between varying axes that represent local area minima to explain the difference observed in the areas of the tissue. The authors note that this rule is applicable when 'internal and external cues are absent'. This statement has resulted in this rule being abandoned; as the authors note, many factors contribute to the division plane, such as the position of the microtubules within the cell [19]. Experiments by Hammant et al. [10] suggest that the position of microtubules is dependent on the stress that the cell experiences from the outside and the inside, and thus they developed a new division rule which has been considered the leading rule for the last few years.

The impact of these division rules on the topology has been studied in different models. A paper by Alim et al. [11] showed that the division method is essential in how the cell grows,

defining the shape and the growth heterogeneity. The authors showed that random division increased noise within the tissue, but also increased the growth heterogeneity within the tissue. Moreover, the observation was made that the Errera rule (or, in the authors' words, 'shortest path method') and the mechanical stress rules reduce growth heterogeneity as they enforce mechanical feedback by redistributing the stress over the whole tissue. The authors show that the choice of division method changes the topological properties within the tissue, which will also be a goal for this paper [11].
A more recent study by Long et al. [20] extended on the mechanical and physical properties of the cell and the effect of this on tissue topology. In their model, the choice was made to incorporate waterflux into the model as the growth mechanism, to simulate this process in biology and confirm a link between pressure and tissue topology. In this model, the authors have shown different relations to be true in their model: not only was the Lewis law experimentally discussed, but the authors also describe the anticorrelation between turgor pressure and cell properties. The turgor pressure in a cell negatively correlates with cell area and also negatively correlates with neighbour number, implying that smaller and low neighbour number cells have a higher turgor pressure than their bigger and higher neighbour number counterpart. An extension was made in the model to couple turgor pressure and growth, as discussed in earlier research by Cheddadi et al. [3], enabling the researchers to make the discovery that the correlation is based on which process is more limiting in the tissue, where they implemented two different regimes: a wall limiting regime, where the walls yield more easily and a flux limited regime, where the water uptake is limited. These regimes showed different signs for the correlations, enabling the different behaviours within the model [20]. However, the researchers have not experimentally tested the effect of the division rules on this model and its properties, and such will be investigated in this paper.
In this study, we will use the vertex model virtualleaf [12] to model cell tissue and the effect of the waterflux on the tissue topology with the respective dividing rules. For the backbone of the waterflux model, a mathematical model made by Cheddadi et al. [3] will be used to build the extension of virtualleaf. This backbone was also used in previous literature, and such should be a well-polished method [3] [20]. In Section 2, virtualleaf, the extension with the waterflux for the model and the dividing rules will be discussed. In Section 3, the results will be presented: Firstly, a study of the current virtualleaf model and the cell geometry will be done. Secondly, the waterflux model will be introduced in a simple two-cell model to investigate the behaviour of the cells with this addition, as well as a wall manipulation study. Lastly, a larger multicellular tissue will be examined with the waterflux extension and the different division rules. To conclude, Section 4 will introduce the conclusion and discussion points on this paper, including the limitations and potential extension to the model.

2 Methods

The model that is used in this paper is virtualleaf. In this model, each cell is described as a set of nodes connected by vertices, more formally written as $C_i = \{V_i, E_i, \alpha_i\}$. The set of n vertices, defined as $V_i = \{v_1, \ldots, v_n\}$ are connected using m edges, which are defined as $E_i = \{e_1, \ldots, e_m\}$. Furthermore, we have a set of cell attributes, which is defined as α_i. In tissue, cell may share the same vertices and edges so we can write the tissue $T = \{C, V, E\}$, where C is the set of the aforementioned cells, $V = \bigcup_{i \in T} V_i$ and $E = \bigcup_{i \in T} E_i$ are the sets of the vertices and the edges respectively. Each of these cells is found on a mesh in a 2D space

on a Cartesian coordinate system [21].
The biological forces in the tissue are engineered by a Hamiltonian in the form of:

$$H = \lambda_A \Sigma_i (a(i) - A_T(i))^2 + \lambda_M \Sigma_j (l(j) - L_T(j))^2 \tag{1}$$

The Hamiltonian in Equation 1 is divided into two constraints: firstly, the cell area constraint, which is defined based on the cell's resting turgor pressure with the target area A_t and the current cell area a. The second part of the Hamiltonian, the wall constraint, which consists of the resting cell wall length L_t and the current cell wall length l, is in conjecture with Lockhart's equation, which states that the walls elastically counteract these forces and the walls can stretch until a certain threshold. The two Lagrange constants in the equation, λ_A and λ_M, determine the cell's resistance to compression or stretching and the spring constant of the cell walls, respectively. This Hamiltonian is minimised using the Metropolis algorithm, which consists of two steps. A simplified overview of this algorithm is shown in Figure 1. At first, the algorithm will try to move a randomly chosen node in a randomly chosen direction using the formula

$$\vec{x}_{new} = \vec{x} + \xi \vec{r} \tag{2}$$

where $r = \{\rho, \theta\}$ is a random vector within the unit circle with the pre-defined algorithm step size ξ. The second step consists of recalculating the Hamiltonian and then the energy difference ΔH. If the energy decreases, the algorithm will always accept the step, and if the energy increases, the algorithm will accept the step using the probability described in Equation 3:

$$\begin{cases} 1 & \textit{if } \Delta H < 0 \\ \exp\left(-\Delta H / T\right) & \textit{if } \Delta H > 0 \end{cases} \tag{3}$$

where T stands for the Boltzmann temperature, allowing some noise in the model and preventing the model from getting stuck in local minima. After trying all the nodes, the last step of the algorithm is to check if the Hamiltonian is below the relaxation threshold θ_h. If not, the algorithm will again try to move the nodes, and if it reaches a correct state, the system is considered to be in equilibrium.

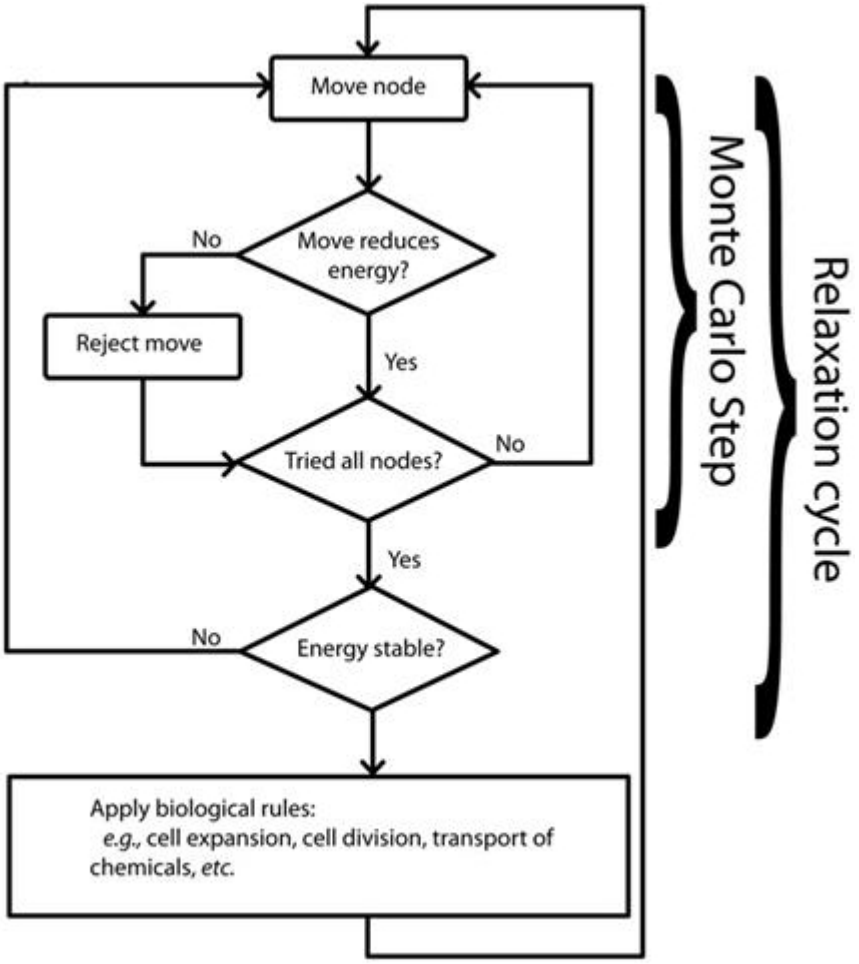

Figure 1: A simplified schematic of the Metropolis algorithm. Image from the paper by Merks et al. [12].

2.1 Expansion of waterflux

Lockhart described the intake of water using the equation

$$\frac{dV}{dt} = AL^a(\Psi_{ext} - \Psi) \tag{4}$$

where the water is described as a flux through a semi-permeable membrane, with the membrane having surface A and permeability L^a. The cell water potential Ψ is calculated as

$$\Psi = P - \pi \tag{5}$$

where the hydrostatic pressure P tends to expel water and osmotic pressure π, which tends to attract water into the cell, which in the case of a single solute of concentration c, can becalculated using $\pi = RTc$. where R is the ideal gas constant and T the temperature. [3]. In the case of our model, we want to split the fluxes into two separate flows: the symplastic and apoplast flux. This model was designed for one elongating cell, so to extend this model into a multicellular model, we have to extend Equation 4 into this context, where we model the water uptake for cell i:

$$\frac{dV_i}{dt} = A_i L_i^a (P^M - P_i) - \sum_{j \in n(i)} A_{ij} L_{ij}^a (P_j - P_i) \tag{6}$$

On the left side of the right part of the equation, the asymplastic flux is calculated roughly the same as in Equation 4; however, the water potential is defined differently. Instead of the potential inside and outside of the cell, the maximum turgor pressure P^M is used to calculate the maximal water uptake. We also assume that the water can move freely in the apoplasm space, as there are experiments that indicate that the extracellular space is not limiting the water movement [22]. On the right side, the symplastic flux is described as a sum over all neighbours $n(i)$ of cell i and the wall surface A_{ij} they share with permeability L_{ij}^a. We make another assumption here, as we take the aforementioned osmotic pressure π to be constant.

2.2 Dividing mechanisms

In this study, two different division rules will be studied. In the next sections, each of these division rules will be expanded on.

2.2.1 Errera's rule

The division over the shortest axis, as described by Errera [17], is already implemented within the current version of virtualleaf. To do so, virtualleaf calculates the inertia tensor and determines the shortest axis of the cell to place the new cell wall. We can define any cell in virtualleaf as an n-sided polygon, which we can use to calculate the moment of inertia tensor, which can be noted as:

$$I = \begin{bmatrix} I_{xx} & I_{xy} \\ I_{yx} & I_{yy} \end{bmatrix} \tag{7}$$

where the individual inertia tensors are calculated using the triangulation of the polygon, where the vertex between two nodes forms the opposing side. This results in the separate calculation:

$$I_{xx} = \Sigma_{i=1}^{n}(y_i^2 + y_i y_{i+1} \cdot A_i) \tag{8}$$

$$I_{yy} = \Sigma_{i=1}^{n}(x_i^2 + x_i x_{i+1} \cdot A_i) \tag{9}$$

$$I_{xy} = (x_i y_{i+1} + x_{i+1} y) \cdot A_i \tag{10}$$

and A_i is the area created by the triangulation of the two nodes.
From this tensor, the largest eigenvalue is calculated and describes the longest axis over which the cell will divide. This tensor is then rotated 90 degrees to calculate the shortest axis.

2.2.2 Random division

The division over the random axis is discussed in the protocol of virtualleaf [23]. The random division is similarly implemented in this study. At every division cycle, the program chooses a random angle using Knuth's subtractive method. In this angle, the new cell wall will be placed.

2.3 Observables

As indicated in Equation 1, the left part of the Hamiltonian represents the area constraint of the cell. We can use the derivative of that to calculate the turgor pressure in the cells, which becomes the following equation:

$$P_i = 2\lambda_a(A_T(i) - a(i)) \tag{11}$$

where P_i stands for the pressure within cell i with the target area A_T and the current area $a(i)$, where the pressure over the whole cell is uniform, as the volume conservation is placed on the whole cell. A negative sign means the cell is able to relax the walls, a positive sign means the cell is under pressure [24].
The right part of the Hamiltonian represents the aforementioned wall length constraint. Using the lengths of the walls, which are being tracked in the model, we can calculate the circumference by summing up the vertices that form a cell. The area of the cell is determined using the same information, as we know the position of the nodes. The shoelace formula makes it possible to calculate the area of an n-sided simple polygon using a counter-clockwise sorted sequence of points. Using the triangulation formula that is defined as:

$$A = \frac{1}{2} \sum_{i=1}^{n} (x_i y_{i+1} - x_{i+1} y_i) \tag{12}$$

Where x_i, y_i are the coordinates of the nodes that make up the polygon [25]. As all the cells in virtualleaf are defined as a closed convex polygon with a set of vertices and edges, the calculations of the area are defined using this equation.

2.4 Implementation

virtualleaf offers a command-line interface to enable the user to simulate the tissue without entering the graphical interface [23]. For the simulations in this paper, the 2.0.0 version of virtualleaf was used, released on 19 November 2024 (see Section 6.1 for more information)[26][12]. The standard set of parameters is used, except when noted otherwise. The maximum time (*maxT* in virtualleaf) is set to 1000 to ensure a full simulation with all the cells reaching their end state. The XML and PNG storage stride (*xml_storage_stride* and *storage_stride* parameters, respectively) are activated and are captured every 500 and 100 steps. The graphical images of the cells are screenshots with the fluxes mode enabled and the other modes disabled. All the starting states of the simulations are available as supplementary material. A total of 20 repeats is used for each simulation.
The expansion of waterflux has been programmed inside virtualleaf with the use of the plugin functionality of virtualleaf, which empowers user to write their own models and simulate them [23]. The first procedure that has been changed is the assignment of the target area of the cell. The target area, as defined in Equation 1, will be defined by the amount of water in the cell, which is defined as a chemical in the model. The amount of water, established as chemical 1 in the model, is a variable of each of the cells in the tissue. When the cell divides, it will divide the water equally between the daughter cells. Inside the plugins, the cell's housekeeping, which will be performed in the last step of the algorithm as described in Figure 1, the interaction with the exterior and neighbouring cells can be modelled, facilitating the modelling of the fluxes. In Section 2.1, the fluxes for one cell are described in Equation 6, which is implemented in the following way: firstly, the first part of the right side of Equation 6 can be calculated under the *CellDynamics* function, where the intake of water from the asymplastic flux can be calculated from the theoretical apoplast. Again, the maximum turgor pressure is defined as 100, as well as the value being divided by 10000, to prevent this part of the equation from taking over the waterflux, as otherwise the cells would only shrink, which has been experimentally defined. The wall length and surface area can be obtained from virtualleaf code. Secondly, the second part of the right side of Equation 6 can be computed under the *CellToCellTransport* function, which handles the flux between two cells that share a wall or interface.

3 Results

3.1 Exploring tissue topology without the waterflux implementation.

3.1.1 Tissue growth shows a similar two phase pattern between division methods.

To test which effect the different division rules have on tissue topology and pressure, the division methods were simulated from the virtualleaf default starting position, shown in Figure 2. In the upcoming section, the pressure, area and number of neighbours will be reviewed in a similar procedure as in the paper by Long et al. [20], where the correlation between the area and the number of neighbours, pressure and number of neighbours and the pressure and area will be discussed.

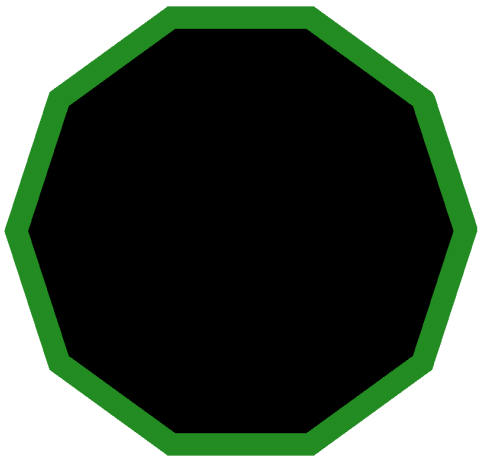

Figure 2: The default starting state in virtualleaf, where the simulations will start from.

In Figure 3, an example of the end state of the three different division methods is shown, after 4000 timesteps. The end states show almost no difference in shape, as both end states are shaped in a circular form. However, we see that the edges of the random division are rough compared to the edges of the Errera division end state. Another argument that the shapes look alike is the radial growth, as the assumption that is used in virtualleaf generates this tissue. An interesting detail is the shape of the cells in the tissue in the end state: all the cells have a round-like shape, but not all are as round as others. In the border regions of the tissue, cells have a more elongated shape, whereas the cells in the middle of the tissue look flattened. This shape and position within the tissue are thus key to different properties, as expected, which will be discussed later.

In Table 1, we can also see that there are small differences between the number of neighbours, pressure and area on average. In total, 20 simulations were done, and the t-tests were performed on the 20 independent averages. The table shows that the difference in the number of neighbours and area is noticeable, as the number of neighbours differs significantly. The same is shown for the average pressure of the cells in the simulations, where the Errera model has significantly lower pressure. However, the area of the cells does not seem to differ.

(a) (b)

Figure 3: End states of the generation of tissues using the different division mechanisms. (a)The end state of a cell with the Errera division procedure. (b) The end state of a cell with the random axis division procedure.

In Video 1, the growth process of tissue is shown using Errera's rule. As can be seen, the growth has different phases, where all the cells divide at once and where all the cells grow. This is expected due to the assumption the model makes, where all the cells have a constant growth rate and consequently give the round shapes that are visible in Figure 3. It is even more visible when the normalised pressure for each cell is plotted, as illustrated by Figure 4; the graphs show the cells' centroids, coloured according to the amount of pressure. A bluer shade of colour implies a cell which is in a relaxed state, while a redder shade of colour implies that the cell is under pressure. In each of the division methods, we can observe that there is a 'division' and 'growth' phase. For example, Figure 4a shows that not all the cells on the outside of the tissue are under stress. However, the cells in the middle of the tissue are under pressure, as expected if the cells are all surrounded by other cells. The end states of the cells have just finished dividing and are thus in a 'growth' phase. In the 'division' phase, the pressure of the cells in the middle is released by dividing, distributing the pressure over the daughter cells. This also poses more pressure on the cells between the outside cells and the divided cell, giving a ring-like shape to the pressure. As shown in Figure 4d, the other division method also shows these phases, which are in line with observations made by Hofler et al. [18], who also report a ring-like stress in radially growing tissue. To further support these findings, the growth of the random axis division can be seen in Video 2.

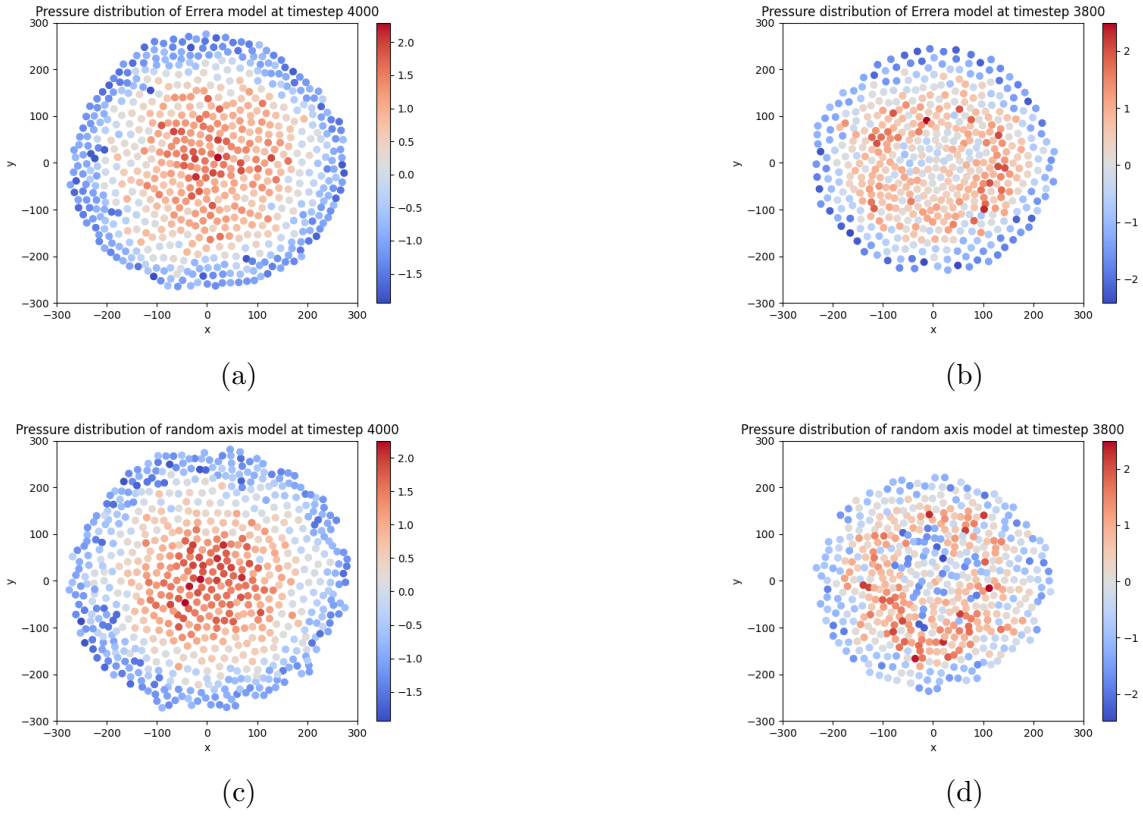

Figure 4: The 'growth' and 'division' phase of the basic model. (a) 'Growth' phase of the Errera division model. (b) 'Division' phase of the Errera division. (c) 'Growth' phase of the random division. (d) 'Division' phase of the random division.

	Number of Neighbours		Pressure		Area	
Model Type	Average	standard deviation	Average	standard deviation	Average	standard deviation
Errera model	6.20	0.02	320.04	126.97	370.24	87.71
Random axis	6.49	0.01	313.29	127.02	371.64	97.36
t-test	$t = 3.64,\ p = 2.7e-4$		$t = 3.63,\ p = 2.7e-4$		$t = -1.10,\ p = 0.2$	

Table 1: Number of Neighbours, Pressure and Area of 20 simulations of each model.

3.1.2 virtualleaf experimentally overshoots the perfect number of neighbours.

To have a more in-depth view of the topology of the tissue, the first notion of Lewis will be discussed [27]. In Figure 5 the neighbour distribution is shown, with the number of neighbours plotted on the x-axis, which can also be seen as the number of edges a cell has, as each edge interface of the cell is shared with another cell and the average amount of cells per simulation on the y-axis over 20 simulations. As in line with Lewis' observation, most of the cells have 6 neighbours, also satisfying Euler's principles as argued by Gibson [9]. Table 1 confirms the suspicion that the average number of neighbours is bigger than 6, overshooting the perfect number of neighbours in an infinite tissue. This may be because of the shape and the position of the cells, as discussed earlier. In the tissue in Figure 3, the cells in the middle of the tissue can be seen to have more neighbours. The opposite is found at the border region, where the cells tend to have fewer neighbours. Together with the fact that the tissue divides in a 'ring' shape fashion, it should be expected that the model has a bit more than 6 neighbours

on average, as the ring also pushes cells inwards, where there are more cells and thus more neighbours on average.

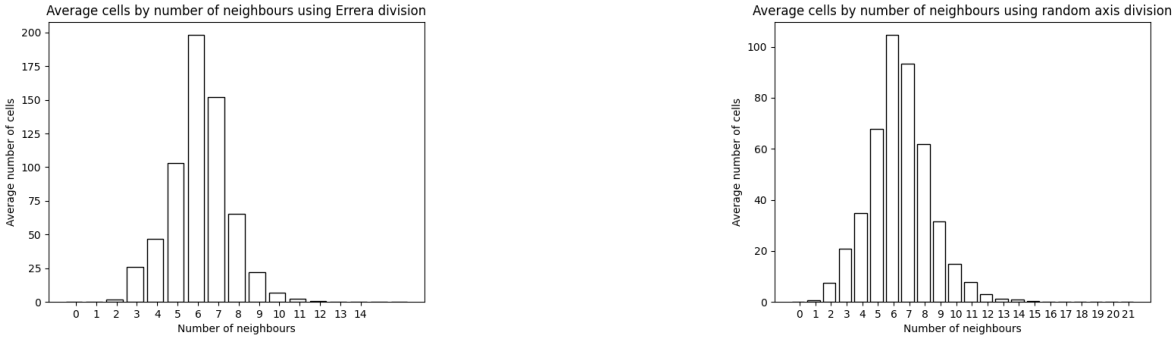

(a) (b)

Figure 5: The number of neighbours on average for each division procedure. (a) The average neighbour distribution of the end state tissue with the Errera division rule procedure. (b) The average neighbour distribution of the end state tissue with the random axis division procedure.

3.1.3 The Lewis law is not adhered to by virtualleaf.

To confirm the Lewis' law introduced in Section 1, the number of neighbours a cell has is plotted against the normalised area of the cells. In Figure 6, the results are plotted, with the number of neighbours on the x-axis and the normalised area on the y-axis, calculated by taking the average area of all the cells within the tissue. The bottom of the box represents the first quartile, the middle line the median and the top of the box the third quartile. The spread outside this box is represented by the whiskers, which show an outlier by 1.5 times the first and third quartiles. The outliers outside of these are represented with hollow dots.
The choice was made to only show the range of neighbours which have a representable amount of cells in each simulation, which was chosen to be the range of 4 to 8. Figure 6a and 6b are the distributions in the end state, and Figure 6c and Figure 5b are the 'division' states.
In Table 2, the Pearson coefficient, p-value and r^2 value are shown to investigate this potential linear relationship.
The table shows that only in two different phases of each of the division methods, in the Errera division phase and the random axis growing phase, there seems to be a somewhat linear relation between the number of neighbours and area. The table also shows that the number of neighbours explains the variance in the normalised area very weakly for all the phases, showing that there may be other factors more dependent than the number of neighbours. However, for the other two phases, the Errera division phase and the random axis division phase, the coefficient illustrates no correlation, supported by the p-value.
Another important data result shown by the graphs is the large spread in the data, making the observations in Table 2 explainable, as the large spread in the data suggests no explicit trend in the data. More interesting, in Figure 8b, the graphs show a lot of outliers, illustrated by the hollow dots, noting that the random axis model is noisier as opposed to the Errera model, due to the random division it makes.

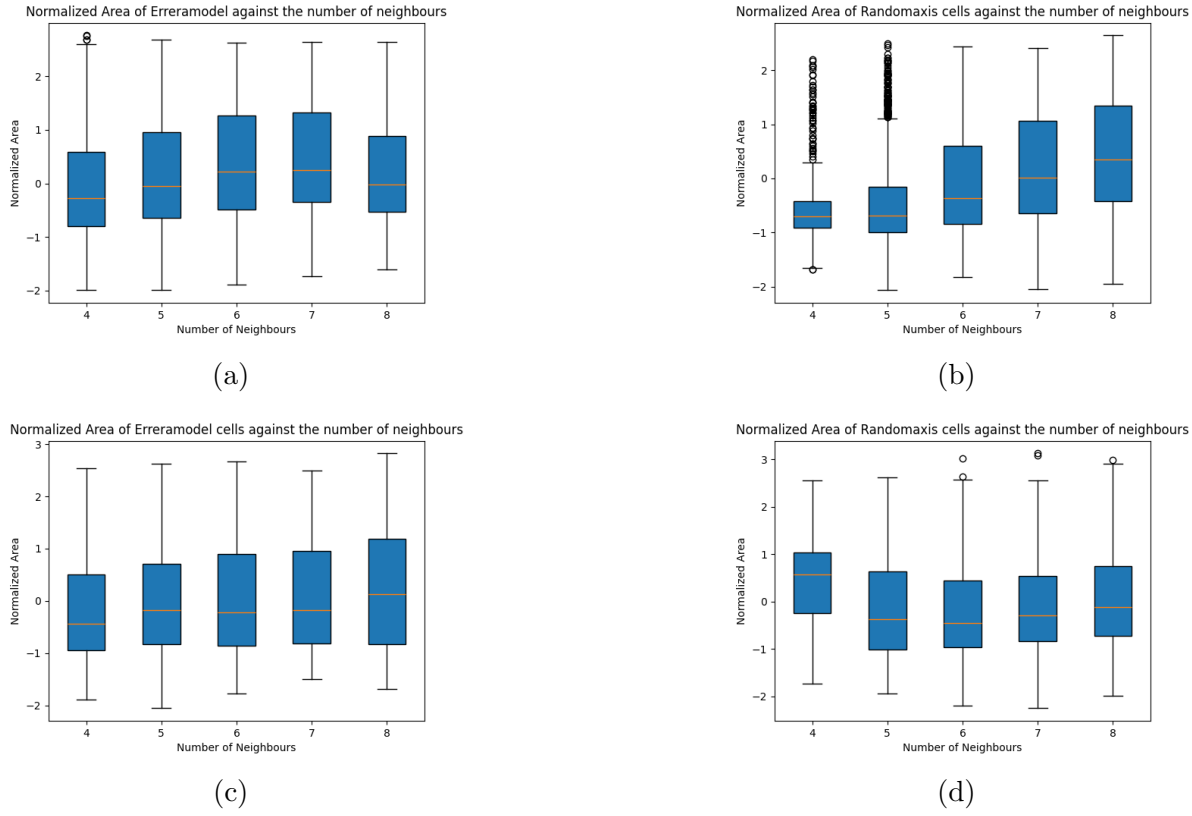

Figure 6: The normalised area plotted against the number of neighbours for each division model in the end state, over 20 simulations each. (a) The normalised area plotted against the number of neighbours for the Errera model in the end state. (b) The normalised area plotted against the number of neighbours for the random axis model in the end state. (c) The normalised area plotted against the number of neighbours for the Errera model in the last 'divide' phase before the end state. (d) The normalised area plotted against the number of neighbours for the random axis model in the last 'divide' phase before the end state.

Model	Phase	Pearson coefficient	p-value	r^2
Errera model	Growing	1.80e-3	0.87	3.23e-6
	Dividing	0.32	1.75e-262	1.02e-1
Random division	Growing	0.34	7.25e-216	0.12
	Dividing	0.02	0.12	3.71e-4

Table 2: The Pearson coefficient, p-value and r^2 value for each of the relations between the normalised area and the number of neighbours for each division method and phase.

3.1.4 Neighbour number weakly explains increment of cell pressure.

Another interpretation for the number of neighbours was made considering the pressure of each of the cells. The normalised pressure, normalised over the average of the total pressure of each cell, is plotted against the number of neighbours in Figure 7. A negative pressure means that the cell is able to relax the walls of the cell; a higher number means the cell is under pressure. The bottom of the box represents the first quartile, the middle line the median

and the top of the box the third quartile. The spread outside this box is represented by the whiskers, which show an outlier by 1.5 times the first and third quartiles. The outliers outside of these are represented with hollow dots.
Again, the choice has been made to show only the number of neighbours that range from 4 to 8 for the aforementioned reason. In Table 3, the Pearson correlation is calculated for each of the division methods and the phase. As well as the coefficient, the p-value and the r^2 are shown.
The figures show that there is a small increase of pressure with the increase of the number of neighbours; the biggest increase can be seen in the random axis model, where there is a big different between the average pressure of the 4 neighbours and the 8 neighbours cell, which is also shown by the Pearson correlation coefficient in Table 3. Moreover, the p-value illustrates that there is some correlation to be found. However, the low r^2 demonstrates that the number of neighbours weakly explains the variation in the normalised pressure. Moreover, the models show a lot of outliers for the cells with 4 neighbours, captivating cells with a higher pressure than the cells on average. This shows that there are cells that are under high pressure despite not having a lot of neighbours, which can be explained by the fact that cells with less neighbours are commonly found at the edges of the tissue (see Figure 3), where the low pressure around the edges can be seen in both phases in Figure 4, as they are not being put under the pressure by the environment, due to virtualleaf not enforcing any stress or pressure from the environment. These outliers are the cells which are not in the outside ring but are instead found inside the tissue. All the plots show a big spread in values, where the biggest differences are seen between the 4 and 5 neighbours. From 5 neighbours on, the pattern is different; smaller differences between the averages and a smaller spread of the values show that these cells are more homogeneous than the cells with a smaller number of neighbours. This can also be caused by the fact that there are more cells on average with that amount of neighbours (as shown in Figure 5). The phase in which the tissue shows a difference in this pattern. This big spread also coincides with the low r^2 values, as the high spread in the data makes it difficult to interpret the correlation.

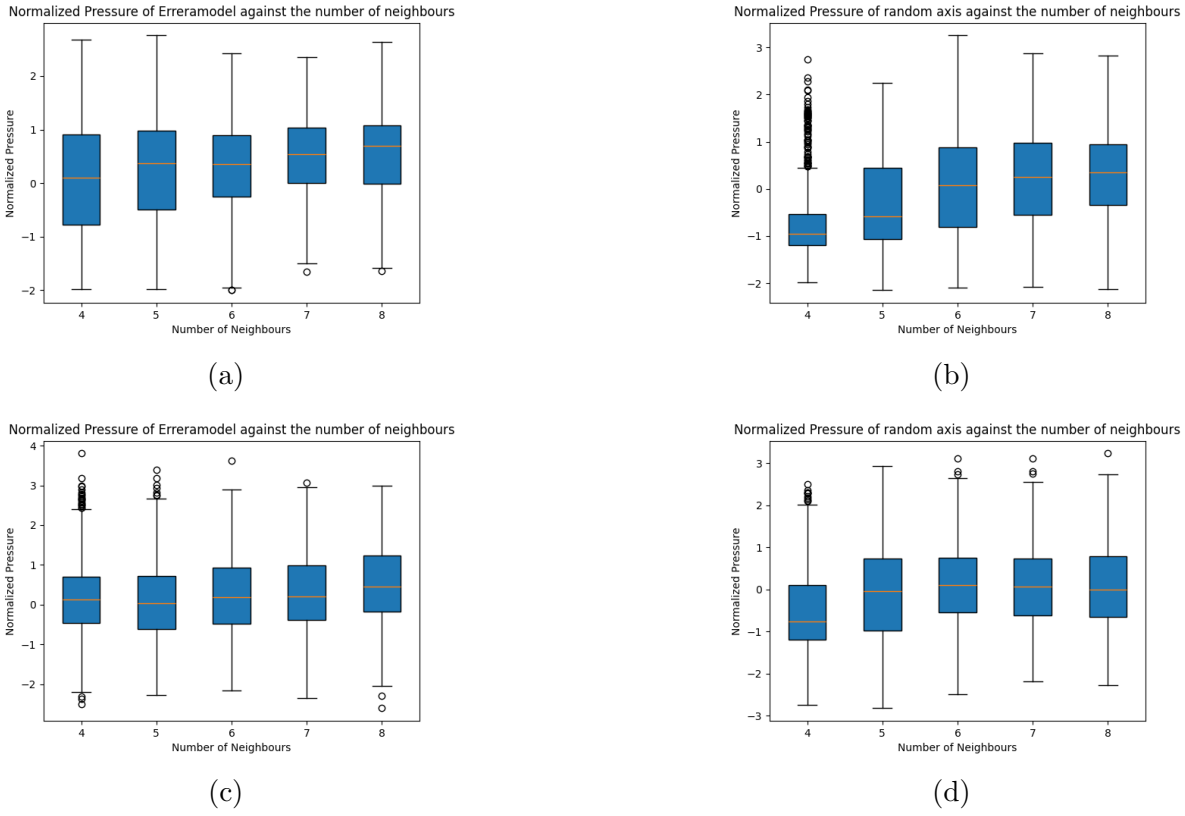

Figure 7: The normalised pressure per number of neighbours for each division method and phase, averaged over 20 simulations. (a) Normalised pressure per number of neighbours for the Errera division in the 'growth' phase. (b) Normalised pressure per number of neighbours for the random axis division in the 'growth' phase. (c) Normalised pressure per number of neighbours for the Errera division in the 'division' phase. (d) Normalised pressure per number of neighbours for the Errera division in the 'division' phase.

Model	Phase	Pearson coefficient	p-value	r^2
Errera model	Dividing	0.20	1.90e-75	0.04
	Growing	0.30	2.16e-225	0.09
Random division	Dividing	0.34	7.25e-216	0.12
	Growing	0.30	1.72e-162	0.09

Table 3: The Pearson coefficient, p-value and r^2 value for each of the relations between the normalised pressure and the number of neighbours for each division method and phase.

3.1.5 Area and pressure relations differ per phase.

To further investigate the pressure of the cells, the plots in Figure 8 show the normalised area plotted against the normalised pressure, both normalised by dividing by the total mean area and mean pressure, respectively, in a scatterplot. The graphs show that the cells are grouped into two different clusters in both the phases and the division methods. In the 'growth' phase, the cells are clustered into a group of small cells with low pressure and a cluster with a varying size but with high pressure. In the 'division' phase, the clusters are reversed, which should be the case: the cluster with large cells under large pressure are the dividing cells and the other cluster are the resting cells, as shown in Figure 8c and in Figure 8d.

To investigate the correlation between the two variables, in Table 4, the Pearson coefficient is shown for the clusters together, showing a negative correlation for the dividing phase, but a positive correlation for the growing phases. This looks to be the very opposite in the graphs. A re-evaluation was done by splitting the cluster by spectral clustering using Scikit learn [28] and re-running the Pearson coefficient tests.
The clusters are shown in Figure 9 and the accompanying coefficients are shown in Table 5, which show different numbers than the coefficients in Table 4. A negative correlation is confirmed, but in the clusters themselves, the correlation is very strong, with the exception of cluster 1 in both of the division phases. The r^2 shows that within the clusters with a negative Pearson coefficient, almost half of the variance in the normalised pressure can be captured by the normalised area, but it is different per cluster. In the Errera division in the growth phase, cluster 1 is better explained by the normalised area than cluster 0, while in the Random axis division in the growth phase, this is the other way around. In the division phase, we see that only in cluster 0 the variance in the area is partly explained by the pressure.
This is very interesting as compared to the model in Long et al. [20], where the authors also found a negative correlation between the area and the pressure, but with the water flux model.

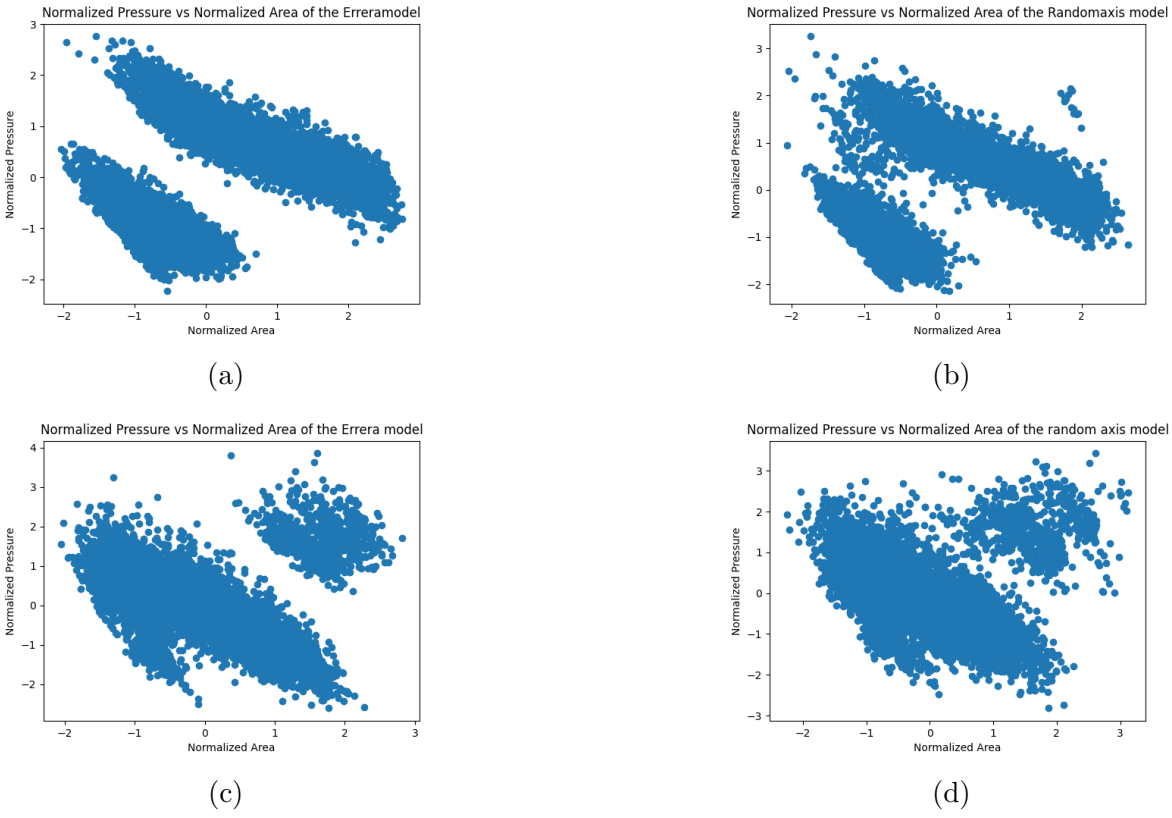

Figure 8: The normalised pressure plotted against the normalised area for each division model, over 20 simulations. (a) The normalised pressure plotted against the normalised area for the Errera model in the 'growth' phase. (b) The normalised pressure plotted against the normalised area for the random axis model in the 'growth' phase. (c) The normalised pressure plotted against the normalised area for the Errera model in the 'division' phase. (d) The normalised pressure plotted against the normalised area for the random axis model in the 'division' phase.

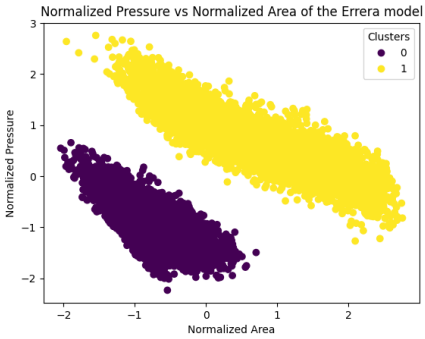

(a)

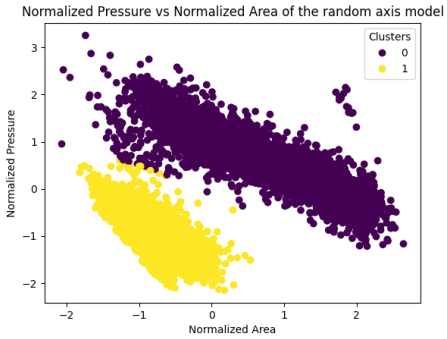

(b)

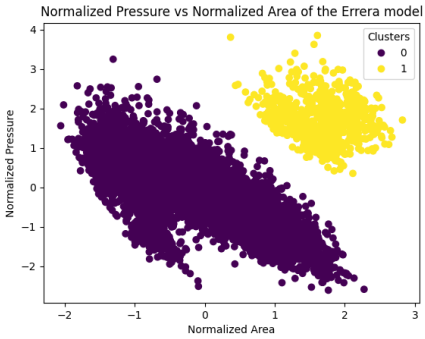

(c)

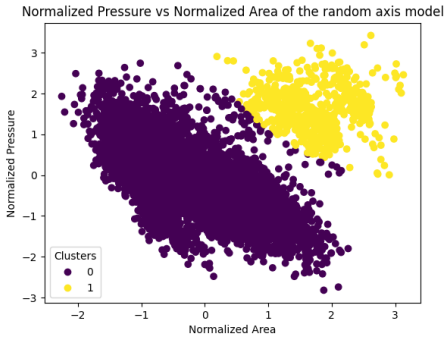

(d)

Figure 9: The new cluster approximated by the spectral clustering algorithm. (a) The clustering for the two clusters for the Errera division procedure in the 'growth' phase. (b) The clustering for the two clusters for the random axis division procedure in the 'growth' phase. (c) The clustering for the two clusters for the Errera division procedure in the 'division' phase. (d) The clustering for the two clusters for the random axis division procedure in the 'division' phase.

Model	Phase	Pearson coefficient	p-value	r^2
Errera model	Dividing	-0.19	2.34e-68	0.04
	Growing	0.20	1.61e-113	0.04
Random division	Dividing	-0.18	1.40e-57	0.03
	Growing	0.2	4.08e-85	0.04

Table 4: The Pearson coefficient, p-value and r^2 value for each of the relations between the normalised pressure and the normalised area for each division method and phase.

Model Type	Phase	Cluster	Pearson Coefficient	p-value	R^2
Erreramodel	Growth	0	-0.72	0	0.52
		1	-0.89	0	0.79
	Division	0	-0.71	0	0.52
		1	-0.18	1.28e-5	0.03
Randomaxis	Growth	0	-0.87	0	0.77
		1	-0.71	0	0.50
	Division	0	-0.68	0	0.46
		1	-0.09	1.26e-3	8e-3

Table 5: The Pearson coefficient, p-value and r^2 value for each of the relations between the normalised pressure and the normalised area for each division method and phase, divided over the clusters as shown in Figure 9

3.1.6 Conclusions on the topology of the virtualleaf model.

In this chapter of the paper, various topological properties of the virtualleaf model have been studied and discussed. The model generates a distribution that resembles that of tissue in nature, with a variety of different cell shapes and sizes, but the other data show that the spread of the pressure and the area is so large, that it is difficult to make conclusions about the concrete relations between the pressure and number of neighbours and the area of the number of neighbours, as compared to the study done by Long et al. [20], who succeeded in showing a negative correlation between pressure and number of neighbours and a positive correlation between the area and the number of neighbours.
However, it is shown that virtualleaf might be able to capture the relation between area and pressure, like the model made by Long et al. [20], showing a negative correlation inside clusters, resembling the negative correlation in the paper.

3.2 Analyzing the effects of the waterflux implementation.

3.2.1 Waterflux pressure introduces different behaviours in a two-cell model.

To capture the effect of the waterflux on the tissue as in nature, the virtualleaf model will be expanded with waterflux application as discussed in Section 2. This addition is the next step in the development of virtualleaf to simulate cell growth better in resemblance to nature and to confirm the *in vivo* experiments as in the paper by Long et al. [20] [3].
As described in Section 2, this model is expanded similarly to the model by Cheddadi et al. [3]. The cells' target area is now based on the amount of water in the cell, and the area tries to expand to that target area. The cell can take up or give off water to the neighbours and exterior through their walls, following Equation 4 and grow or decrease following this equation. The ϕ^a and ϕ^s can be proportionally modelled to the permeability L^a and L^s, and the wall extensibility is conveniently calculated in the virtualleaf Hamiltonian as the parameter λ_M (see Equation 1). The osmotic pressure is kept constant.
There are two dimensionless parameters that influence the system dynamics:

- α^s, formally described in the paper as $\alpha_s = \frac{\phi^s}{\phi^a+\phi^s}$, where ϕ^s describes the symplasmic conductivity and ϕ^a the asymplastic conductivity. This results in the parameter characterising the relation between these two parameters, where a value of 0.5 is a balance

between the two, a value below 0.5 an asymplastic dominance and a value above 0.5 a symplastic dominance. This value is bounded between 0 and 1.

- α^a, formally described in the paper as $\alpha^a = \frac{\phi^a}{\phi^w + \phi^a}$, where ϕ^a describes the aforementioned asymplastic conductivity and ϕ^w the cell wall extensibility. This parameter can also be interpreted as the balance of growth control between these two parameters, where a value of 0.5 is an equilibrium between the two, a value below 0.5 indicates more control by cell wall extensibility and a value above 0.5 indicates more control by the asymplastic conductivity.

The first step of the exploration is to start with a simple two-cell model and show the growth behaviour it demonstrates using different parameters. The starting state of the two-cell model is shown in Figure 10, where there are two approximately equal-sized cells with a starting condition of 400 water in each cell and with an endstate at 5000 timesteps. The growth is capped at 1000 units of water to give the best presentation of the water in the cells.

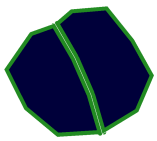

Figure 10: The starting state of the two-cell model. The cells share a wall, where the symplastic fluxes are being calculated.

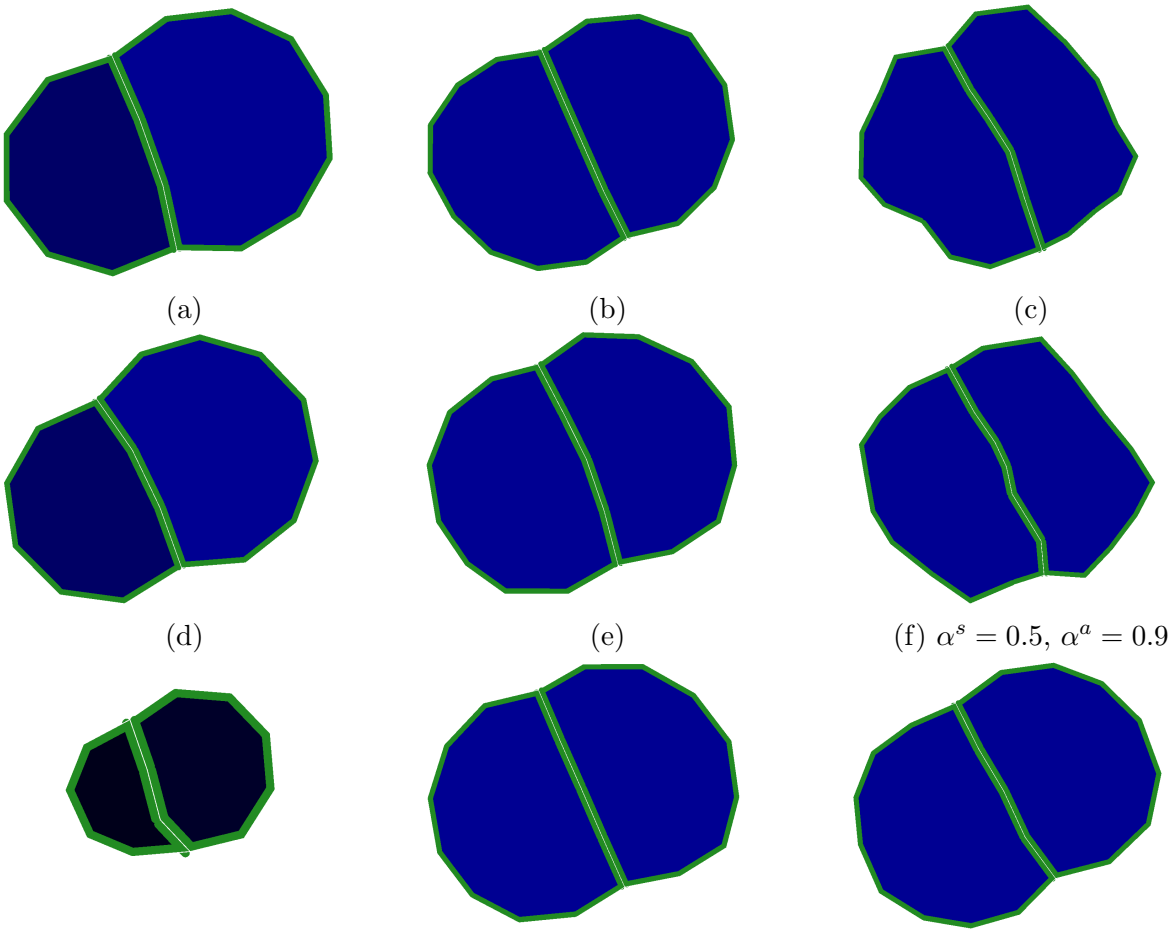

(a) (b) (c)

(d) (e) (f) $\alpha^s = 0.5$, $\alpha^a = 0.9$

(g) $\alpha^s = 0.1$, $\alpha^a = 0.1$ (h) $\alpha^s = 0.1$, $\alpha^a = 0.5$ (i) $\alpha^s = 0.1$, $\alpha^a = 0.9$

Figure 11: The outcome of the two-cell model in 9 different parameter settings as described earlier. The figures are placed such that the α^s value increases on the x-axis and the α^a value on the y-axis. (a) $\alpha^s = 0.9$, $\alpha^a = 0.1$ (b) $\alpha^s = 0.9$, $\alpha^a = 0.5$ (c) $\alpha^s = 0.9$, $\alpha^a = 0.9$ (d) $\alpha^s = 0.5$, $\alpha^a = 0.1$ (e) $\alpha^s = 0.5$, $\alpha^a = 0.5$ (f) $\alpha^s = 0.5$, $\alpha^a = 0.9$ (g) $\alpha^s = 0.1$, $\alpha^a = 0.1$ (h) $\alpha^s = 0.1$, $\alpha^a = 0.5$ (i) $\alpha^s = 0.1$, $\alpha^a = 0.9$

In Figure 11, nine different simulations' end states are shown. On the x-axis, the α^a is increased and on the y-axis, the α^s is increased. The blue tint of the cell is proportional to the amount of water the cell has. In Video 3, the growth of the balanced cell is shown, where both cells grow to be around the same size. When α^a is low, we see that the cells tend to lose a lot of water to their surroundings, as can be seen due to the size of cells in Figure 11a. However, we see that the right cell is significantly bigger than the left cell. This discrepancy in area size is also seen for the other cells in this column, where we see an obvious area difference between the two cells. The complete growth cycle is shown in Video 4, where it can be seen that the bigger cell prevents the smaller cell from growing by acquiring all the water. An outlier is illustrated for the low α^s low α^a case in Figure 11g, where the standard deviation is the highest in the table. A possible explanation may be virtualleaf ability to handle smaller cells (as the cells are comparatively the smallest in terms of area of all the simulations), as the program tends to struggle with smaller areas.
This different ratio between the cell growth is illustrated by the other simulations of the model: in Figure 12, the growth of the area over time can be seen. With a balanced and high α^a, we observe that the cells are almost the same size and are all fairly round in shape and are equally

big, meaning that the walls are not able to relax the turgor. This difference can be clearly seen in cases where the walls are able to relax the turgor, such as in the case of a high α^a, where there is a really low pressure. The unbalanced growth is also shown to have different regimes: in the lower corner, the cell almost completely prevents the cell from growing, while in the other case, the other cell has grown a little bit.
The contrast in pressure is well shown in Table S10, where the pressure varies widely between the differences in α^a, with a high α^a giving a lower pressure, nearing the 0 pressure inside a cell, and a lower α^a giving a higher pressure. There are even cases where the pressure acquires a negative value, in the case the cell has to lose water to its surroundings to lose the pressure. The standard deviation of these simulations is also interesting: the standard deviation in all the cases appears to be very low, meaning that there is not a lot of variance in the repeats of the simulations.

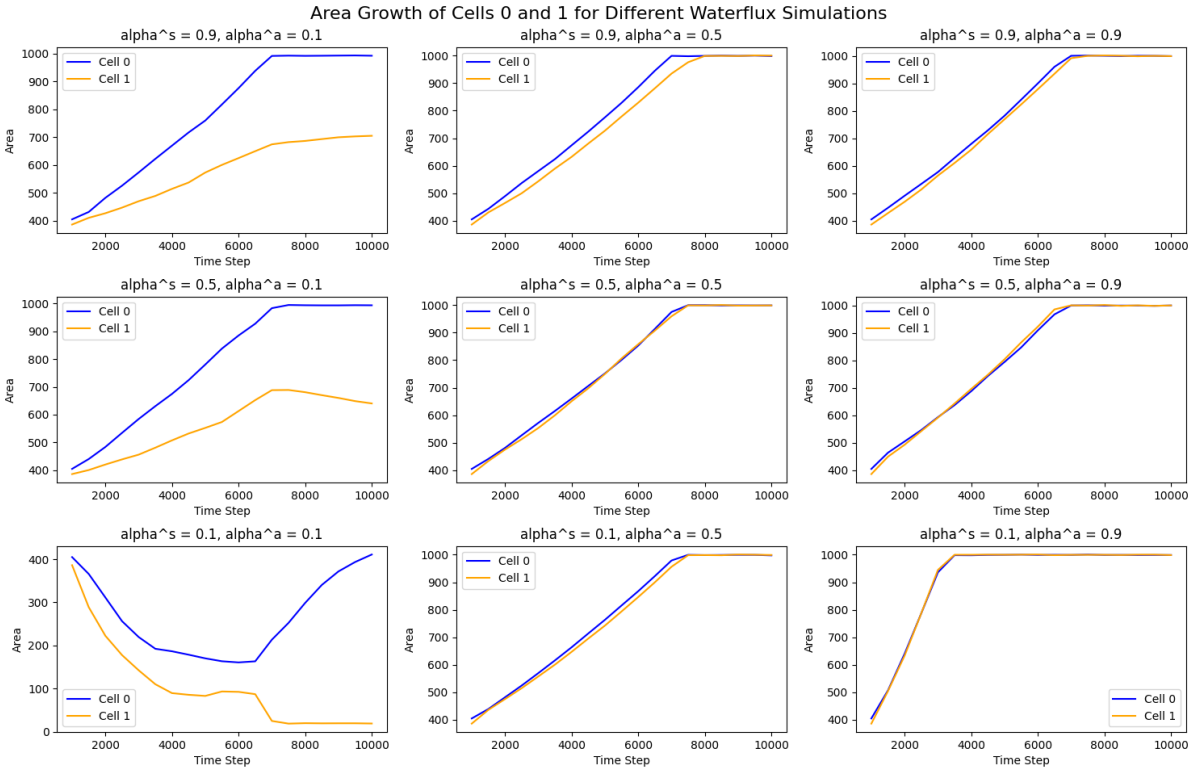

Figure 12: The difference of the area over time

The simulation shows that there are two noticeable categories in the behaviour of the two-cell model that can be defined.

1. A balanced growth, where both the cells grow equally big and the cell walls expand the cell

2. An unequal growth, where one cell prevents the other cell from growing.

To separate these two categories, in Figure 13 a phase plane is sketched on a 0.1 scale for the two-cell model. In Area I, on the left side of the blue line in Figure 13, the two cell models show an unbalanced growth behaviour. In Area II, the balanced cell growth can be found.
The simulations show a somewhat similar pattern to the model in the paper by Cheddadi et al. [3]. In the paper, the authors explain that they also found a set of parameters where the one

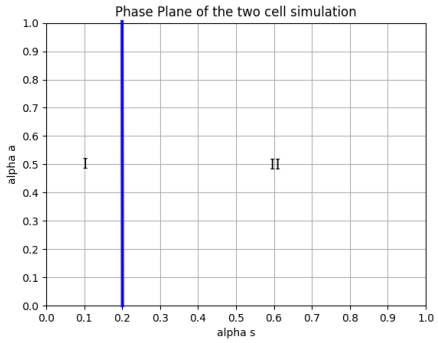

Figure 13: A simple phase plane, where on the x-axis α^s is plotted and on the y-axis α^a. Area I depicts the unbalanced growth area, Area II the balanced growth.

of the cells prevents the other cell from growing and a set of parameters where the two cell methods shows a balanced growing behaviour, but find a different phase plane as compared as in Figure 13, as well as different levels of unbalanced growth in the behaviour, indicating that the simulations of this model in this paper may not captivate the complete complexity of the waterflux model the authors propose [3].

3.2.2 Wall softening causes growth inequalities with certain parameter sets.

In Section 3.2.1 the observation was made that there are different behaviours when it comes to a two cell model, showing similarities to the model of Cheddadi et al. [3] To further encapsulate and compare the model, the model will be extended the same way as the aforementioned paper proposed using a numerical example where the shoot apical meristem is modelled. In earlier studies, it was observed that differences in growth rate can be triggered by the local manipulation of the cell wall mechanics [29]. In the case of a SAM, the observation is made that there are certain bump cells which have a higher growth rate, due to the fact that the walls have a lower elastic modulus. In this experiment, we imitate the setup established by Cheddadi et al.: in virtualleaf, a cell will be grown with Errera division and three cells will be selected, as shown in Figure 14.
The bump cells are marked with a red 'x', where the wall stiffness is halved. Based on the previous observations in this model, the differences in growth rate are most present with a high α^s, representing a high flux between the two cells compared to the symplastic flux and with a low α^a, representing the control of cell wall stiffness. Another argument that has not been explored in detail in this thesis is the role of the outside water potential, described as the osmotic pressure, which has to be set at the correct level to encourage cells to grow. To investigate the effect of growth heterogeneity, we will have two cases where the heterogeneity

is lowered and one where the heterogeneity is heightened, to compare the observations.

- The lower cell-to-cell conductivity set (CC-), where the α^s is set to a lower value, where the expectation is that every cell will grow with the same rate and no difference will be seen with the bump cell. The used parameters are $\alpha^s = 0.1$ and $\alpha^a = 0.5$.
- The higher fluxes control set (ALPHA+), where the α^a is set to a higher value, where the expectation is that only the bump cells will be able to relax the walls by the pressure, but still with high growth rates. The used parameters are $\alpha^s = 0.5$ and $\alpha^a = 0.1$.
- The lower osmosis pressure set (OP-), where the osmotic pressure is lower, to increase the growth rate differences, as a lower cell wall stiffness should enable the bump cells to grow quickly. Instead of the 100 standardly defined in the model, the osmotic pressure will be set to 50.
- a reference set (REF), using a balanced setup of both α^a and α^s. The used parameters are $\alpha^s = 0.5$ and $\alpha^a = 0.5$.

.

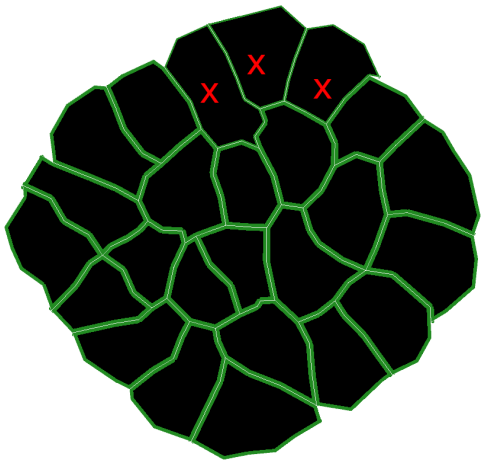

Figure 14: The starting tissue for the numerical examples.

In Figure 15, the results of a single simulation are shown after 10000 timesteps for each of the reference sets. The bump cells are the top cells, which can be seen by the thinner walls that are drawn by the virtualleaf interface. In Figure 15e and 15f, the area and the turgor pressure of the bump cells, respectively, are shown over time for each model, over the 10000 timesteps the tissue has been simulated.
Interestingly, the ALPHA+ and CC- set, Figure 15b and 15a respectively, show that the bump cells did not grow larger than any of the cells in the border region of the tissue. However, all the cells outside of the border region grew less, giving all the cells in the border region a bigger area. In both sets, this behaviour is seen. This is in contrast to the reference and the OP- set, which are represented in Figure 15d and 15c. In the OP- set, the effect of the lower osmotic pressure is visible due to the size of the tissue and the bump cells being smaller than the rest. This is also illustrated in Figure 15e, where the bump cell growth is shown for all the models. The growth for the OP- model is the slowest of all the models, where other models grow their bump cells quickly. The reference set has the highest growth rate, and the ALPHA+ and CC- sets show a similar growth rate with their bump cells.

Comparing this to the model made by Cheddadi et al. [3], there are differences to be noted. The reference set shows similar behaviour, as in the paper, the authors also discuss the bigger area bump cells, as can be seen in Figure 15d. It is interesting that the bump cells have a lower turgor pressure on average than the other cells, which is also discussed by the authors. Moreover, the authors also see the same growth pattern arise with OP- set, where the tissue is smaller and the cells grow more slowly. There is a difference to be seen in the area of the bump cells, where the growth seems to flatten in the virtualleaf model. This could be due to the fact that the authors did not simulate the tissue for long enough to show this drop in growth.
The main differences are the CC- and the ALPHA+ set, as they grow very differently. In the CC- set, the authors show that all cells grow, and the turgor pressure lowers in the bump cells. However, as Figure 15a shows, the virtualleaf model does not adhere to this same behaviour. When the turgor pressure is studied, the bump cells do match up with the observation made by the authors, where the turgor pressure drops over time, as shown in Figure 15f where a small drop of pressure can be seen, but the turgor in the virtualleaf seems to be very unstable as compared to the turgor pressure in the Cheddadi et al. paper [3].
The border heavy growth is also shown by the ALPHA+ set, as shown in Figure 15b. The tissue shows that cell walls are very rigid, as demonstrated by the graphical interface of virtualleaf in the picture. This also shows disparity with the Cheddadi et al. [3] study, as the authors show a less rigid cell, with pronounced bump cells. In the virtualleaf model, the turgor in the bump cells shows a drop, but a more direct drop compared to what was found by Cheddadi et al. [3]. The unstable pressure, mentioned in the CC- set, is also observed here.
However, the reference and OM set lead to a growth pattern which resembles the author's model. The bump cells are very much defined as they grew larger than the other cells, but at different rates, as shown in Figure 15e. The difference in results shows in the turgor pressure, where the turgor pressure of the bump cells in the virtualleaf model remains constant, as can be seen in Figure 15f, but the other cells gain pressure over time, which is the opposite Cheddadi et al. observed. However, the lower turgor pressure in the non-bump cells is a pattern that the authors do recognise. This is also important as the authors propose this mechanism as the flux-based lateral inhibition in their model, which looks to also be present in this model, as the bump cell prevents the other cells from growing [3].

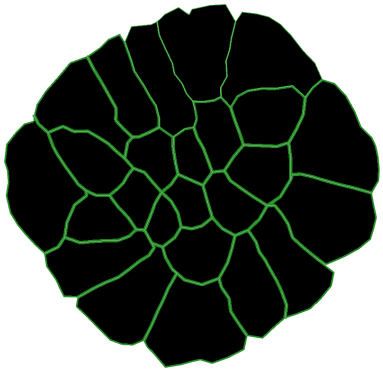

(a)

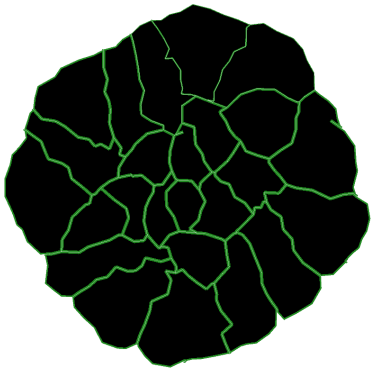

(b)

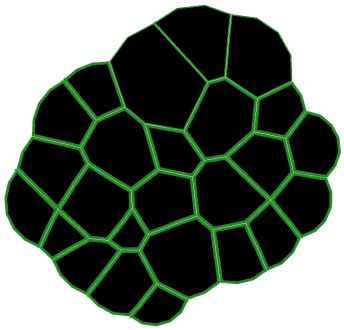

(c)

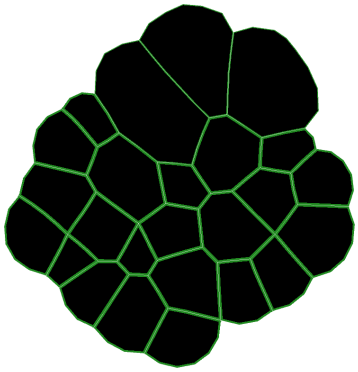

(d)

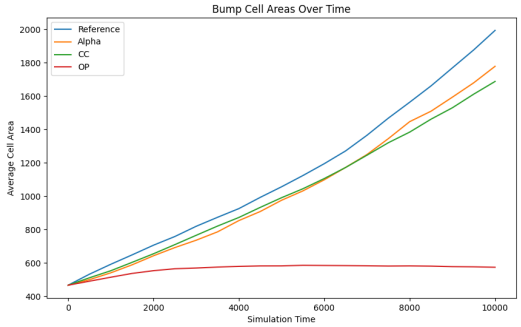

(e)

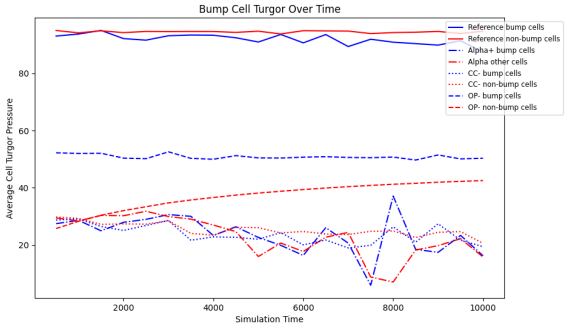

(f)

Figure 15: The end states of one simulation of the bump cell tissue, from the starting point as described in Figure 14. (a) The end state of the CC- set, after 10000 timesteps. (b) The end state of the ALPHA+ set, after 10000 timesteps. (c) The end state of the OP- set, after 10000 timesteps. (d) The end state of the ref set, after 10000 timesteps. (e) Bump cells' average area over time, for each model. (d) Bump cells' and non-bump cells' average turgor pressure over time, for each model.

3.2.3 Conclusions on the analysis.

In this section, we experimented with the waterflux in two different settings, where we got some interesting results compared to the model it was based on. The two-cell model, where we studied two cells growing, shows that there are two different behaviours that arise from the parameter space we have: one where both the cells grow equally and one where one cell grows more than the other, preventing the other cell from growing. This behaviour shows similarity with the Cheddadi et al. [3], where the authors also proposed a phase plane like in Figure 13, but in more detail. Next, we experimented with a simulation proposed by Cheddadi et al. [3], where we studied the wall loosening as observed in the shoot apical meristem, which shows that growth rate differences can be triggered by wall manipulation [29]. Four different parameter sets were tested, and the virtualleaf showed similarities for two different simulations, but showed differences in the other two. However, the possible lateral inhibition feedback observed by Cheddadi et al. [3] may also be present in this model.

3.3 The waterflux model shows different topological characteristics.

3.3.1 Different division methods show dissimilarity in shape and size.

To explore how the waterflux and the division methods affect the topology, the different division rules will be used to grow a tissue using the waterflux addition to the model. Both α^a and α^s are set to 0.5 to ensure a balanced growth in all the cells, as observed in Figure 11e and in Figure 13. Starting from the same starting tissue as described in Figure 10, the tissue was grown over 12000 timesteps, as compared to the 10000 timesteps in Section 3.1.1 to ensure a big enough tissue. Further simulation of the tissue resulted in unstable simulations, so the choice was made to cut off the simulation at that point.

(a) (b)

Figure 16: End states of the generation of tissues using the different division mechanisms using the Waterflux after 12000 timesteps. (a) The end state of a cell with the Errera division procedure using the Waterflux. (b) The end state of a cell with the random axis division procedure using the Waterflux.

In Figure 16, two examples of the end states of the division methods are shown. In the figure, the blue shade represents how much water is in the cell. The first thing that is immediate is the size of the tissue: the waterflux-based model grows slower compared to the model described

in Section 3.1.1. The cells do have the round shape previously observed, but the edges are rougher on all models. At the edges, the cells do not form a smooth boundary, but rather have different sizes and create bumps in the boundary region to the outside. The cell shapes differ widely, with elongated, round and flattened cells at different spots in the tissue. In Video 6, the growth is shown for a tissue with the Errera division method, where there is less of a phase difference to be seen, as cells at different places in the tissue divide, giving a more diverse division pattern and a less heterogeneous growth. There is also a noticeable difference between the division methods, where the division method can be seen to be very different. The best example of this can be seen in the random axis division in Figure 16b, where in the left upper edge, there are really oblongated cells.
The statistics in Table 6 show that the division methods are different over 20 simulations. For the number of neighbours, pressure and area, a t-test is performed to test whether the difference is significant between the averages, and all the differences seem to be significant. This is mainly interesting for the values of the pressure and the average, which have a big spread compared to the average number of neighbours in the previous model in Section 3.1.1, making the difference significantly important.

	Number of Neighbours		Pressure		Area	
Model Type	Average	Standard Deviant	Average	Standard Deviant	Average	Standard Deviant
Erreramodel	5.85	2.32	27.35	27.60	420.53	85.74
Randomaxis	4.67	2.59	30.98	29.24	423.82	82.56
t-test	$t = 13.59,\ p = 4.09e-29$		$t = -5.22,\ p = 5.07e-7$		$t = 5.57,\ p = 5.41e-10$	

Table 6: The average number of neighbours, pressure and area of each of the division methods using the waterflux over 20 simulations.

3.3.2 The waterflux model undershoots the perfect number of neighbours.

To further examine the first observation of Lewis [27], the neighbour distributions are plotted in Figure 17 as well as the average number of neighbours per cell in Table 6. It can be recognised that the average number of neighbours is under 6, the perfect number as attained by Lewis. For the random axis procedure, the number is under 5, further enforcing the random noise. The low number of timesteps done by the simulation may be an explanation for the undershooting of the average, as the number is close to 6 with the number of cells as shown by Gibson et al. [30].
The large standard deviation, as compared to the previous model, where the number of neighbours is portrayed in Table 1, can be well seen in the distributions in Figure 17. Rather than the placement of the distribution to the right of the perfect number 6 in Figure 5, we see a shift to the left. After the count of 6 numbers, the number of cells quickly drops off. The big difference can be explained by how the tissue is being divided; instead of going through the phases as described in Section 3.1.1, the cells divide based on the water pressure, which is more dependent on their neighbours and the water uptake through the apoplast, resulting in lower amount of neighbours on average and a different growing pattern.

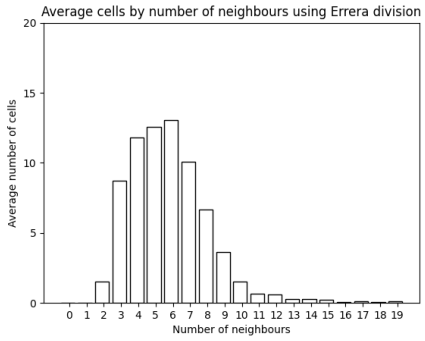

(a)

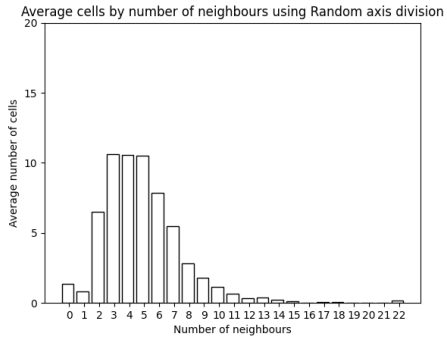

(b) .

Figure 17: The neighbour distribution of the three division methods with the waterflux expansion. (a) The neighbour distribution of cells with the Errera division procedure using the waterflux. (b) The neighbour distribution of cells with the Random axis division procedure using the waterflux.

3.3.3 There is no correlation between area and neighbour number

To test whether the Lewis' law, the linear relation between cell area and number of neighbours, holds, the number of neighbours is plotted against the normalised area in Figure 18. The normalised area is calculated using the average over the whole tissue. The bottom of the box represents the first quartile, the middle line the median and the top of the box the third quartile. The spread outside this box is represented by the whiskers, which show an outlier by 1.5 times the first and third quartiles. The outliers outside of these are represented with hollow dots. The linear relation is again studied by calculating the Pearson coefficient: in Table 7, the Pearson coefficient is calculated. As can be seen in the table, a small correlation is found, but it does not explain the variance very well, as indicated by the r^2 values in Table 7. It is also shown in Figure 18 that no significant trend can be seen, as well as a large spread as seen earlier in the simulation of the previous model (as seen in Section 3.1.1, adding uncertainty to the data. This shows that the data suggests that the Lewis' law does not hold in this model, as compared to the findings of Long et al. [20], who found that in their model, this positive correlation can be found, but with a consistently smaller spread in the data as well.
In comparison with the previous model, the observation seems to match. In the previous model, no significant correlation was also found, confirming that the addition of waterflux does not change the growth patterns across the tissue.

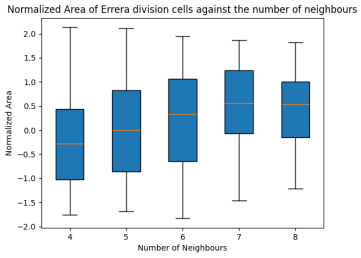

(a)

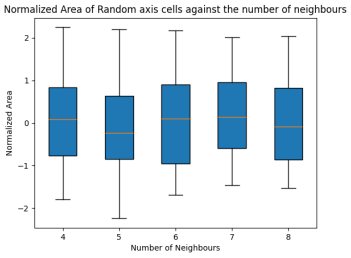

(b)

Figure 18: The normalised area of cells against the number of neighbours for the two division methods with the waterflux expansion over 20 simulations. (a) The normalised area of cells against the number of neighbours for the Errera division procedure using the waterflux.(b) The normalised area of cells against the number of neighbours for the random axis division procedure using the waterflux.

Model	Pearson coefficient	p-value	R^2
Errera model	0.09	2.25e-3	8.06e-3
Random division	0.10	5.66e-3	9.78e-3

Table 7: The Pearson coefficient, p-value and r^2 value for each of the relations between the normalised pressure and the number of neighbours for each division method and phase.

3.3.4 The pressure of the cells does not change much with the neighbour number.

To see whether the pressure correlates with the neighbour number, Figure 19 illustrates the number of neighbours on the x-axis and the normalised pressure on the y-axis. The pressure is normalised by the average over the whole tissue. The normalised area is calculated using the average over the whole tissue. The bottom of the box represents the first quartile, the middle line the median and the top of the box the third quartile. The spread outside this box is represented by the whiskers, which show an outlier by 1.5 times the first and third quartiles. The outliers outside of these are represented with hollow dots.
In Figure 19, the graphs show that the data does not change with the number of neighbours. To confirm this, the Pearson coefficient is calculated in Table 8 as well as the corresponding p-value and the r^2 value. This table shows a very low Pearson coefficient, as well as a p-value indicating that there may be no correlation, as the p-value for the Errera model is higher than 0.05 and random division at 0.03. These values, as well as the boxplots in Figure 19, suggest that there is no relation between the number of neighbours and pressure in the waterflux model.
Compared to the model made by Long et al. [20], this shows a dissimilarity: the model shows a negative correlation between the number of neighbours and pressure. The addition of the waterflux to the model has not been able to replicate this same behaviour.
As compared to the previous model, the aforementioned showed a weakly explained correlation, whereas in this model, there seems to be no better correlation.

(a) (b)

Figure 19: The normalised pressure against the number of neighbours of the two division methods with the waterflux expansion over 20 simulations. (a) The normalised pressure against the number of neighbours for the Errera division procedure. (b) The normalised pressure against the number of neighbours for the random axis division procedure.

Model	Pearson coefficient	p-value	R^2
Errera model	0.05	0.06	3.15e-3
Random division	0.07	0.03	5.55e-3

Table 8: The Pearson coefficient, p-value and r^2 value for each of the relations between the normalised area and the number of neighbours for each division method.

3.3.5 Pressure and area form one cluster

Lastly, Figure 20 shows the normalised area plotted against the normalised area, both normalised by dividing by the total mean area and mean pressure, respectively. In both the division methods, no strong correlation is observed between normalised pressure and normalised area, indicating that pressure remains relatively independent of area in these simulations. This is also confirmed by the Pearson coefficient shown in Table 9. However, the p-value indicates that the correlation may not be 0. The data points are widely dispersed around zero in each plot, with no evident linear or non-linear trend. In the Errera division procedure in Figure 20a, the cells seem to be concentrated near the 0 area of the pressure, but have a large spread between the areas, while the longest axis also seems to have a bigger spread on the pressure axis. Overall, the normalised pressure appears largely uncorrelated with normalised area in all three division models, supporting the conclusion that, within these simulations, cell area is not a strong predictor of pressure dynamics across models.

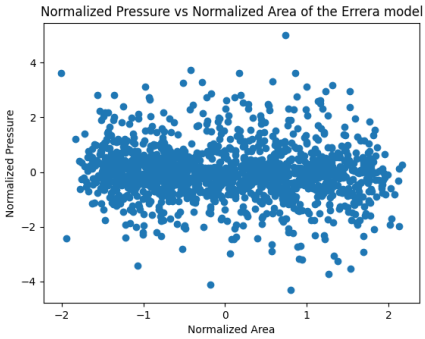

(a)

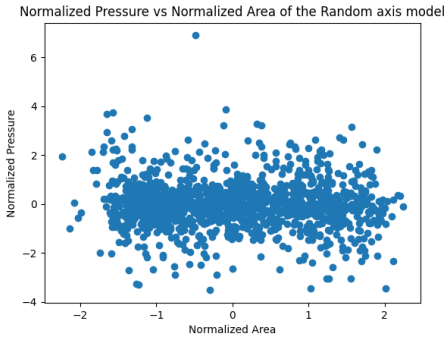

(b)

Figure 20: The normalised pressure against the normalised area of cells with the waterflux expansion over 20 simulations. (a) The normalised pressure against the normalised area of cells with the Errera division procedure using the waterflux. (b) The normalised pressure against the normalised area of cells with the Random axis division procedure using the waterflux.

Model	Pearson coefficient	p-value	r^2
Errera model	-0.08	1.25e-3	7.22e-3
Random division	-0.05	0.04	3.33e-3

Table 9: The Pearson coefficient, p-value and r^2 value for each of the relations between the normalised area and the number of neighbours for each division method.

4 Discussion

4.1 Results

In this paper, we used the virtualleaf model to study the topological properties and the effect of the turgor pressure on these topological properties. Two different division methods were used when growing tissue, to determine the effect of each of these procedures: the Errera division method, which uses the shortest path of the cell to divide and the random division method, which chooses a random division in the cell to divide. We then extended the virtualleaf model with the waterflux as theorised by Cheddadi et al. [3], introducing a new turgor pressure based on the amount of water that is inside a cell, as well as the addition of two parameters which influence: α^a and α^s, which model the relation between the wall synthesis and the apoplasmic fluxes and the relation between the apoplasmic and symplasmic fluxes, respectively. This addition was first tested in the case of a simple two-cell model, where the two parameters were investigated. This was further expanded into a multicellularity context, where an experiment resembling a shoot apical meristem was conducted, to see the effect of wall stiffness on the growth and waterfluxes inside this system. Lastly, the new model was studied in the light of the pressure and topology, with the same two division methods as in the first model.
In Section 3.1.1, we showed that the default virtualleaf model grows a circular-shaped tissue, where the number of neighbours is close to 6, but goes over this number. Calculations also show that there is no significant correlation between the area and number of neighbours and the pressure and number of neighbours, due to the big spread in the data that results from

this model. However, an interesting correlation that does show is within the pressure and area when clustered, which shows a surprising similarity with the model of Long et al.[20].
Section 3.2 describes the behaviour that arises when the waterflux expansion is added; in the default virtualleaf model, this is not implemented, while it is an essential part of the growing and shrinking of the cell area [3]. We show that two different behaviours arise, similar to the model by Cheddadi et al. [3], with an unbalanced growth and a balanced growth behaviour. This paper also illustrates the phase plan on a low level, showing that the similarities are striking. More detailed simulations are necessary to create a detailed phase plane and to compare with the findings by Cheddadi et al. [3], to gain more insight into the virtualleaf model and the workings of the waterflux expansion. In Section 3.2.2, we introduced a multicellular simulation, where we simulated a model based on the shoot apical meristem. In this simulation, three cells inside a bigger tissue had their wall stiffness halved, to trigger growth inequalities [29]. The simulation showed that for two different parameter sets, the cells with halved wall stiffness grew bigger and had different turgor pressure than the cells which did not have this wall manipulation done. However, the simulations also showed differences with the study, where the bump cells did not grow bigger, but the cells in the border region all grew large, while the cells in the middle of the tissue did not. A potential cause may be the low cell-to-cell flux, preventing the middle cell from growing, as they have many neighbours compared to border region cells. Another potential cause may be the size of the cells, as the cell sizes were not all the same, which is a big difference compared to the study done by Cheddadi et al. [3]. However, one of the sets showed the same behaviour that the authors found in a flux lateral inhibition, which shows that the virtualleaf model is able to reproduce this process.
In Section 2.1, the same topology aspects as in the first chapter, but with the newly built waterflux expansion. These results show different values as compared to the default virtualleaf model, as the growth pattern is different. Despite this, the model shows no significant correlation between area and neighbour number, pressure and neighbour number and pressure and area, contrary to the model on which it is based [20].
Moreover, the two-cell dynamic study showed that the simple additions to the model resulted in three different behaviours arising from the different parameter sets: a balanced growth with high and low pressure and an unequal growth, in which one cell grew observably larger and quicker, preventing the other cell from growing. To further explore this mechanism and a possible deeper tissue connection, a soft wall model was studied. These results failed to replicate the earlier observation in the two-cell model, but also the observation made by Cheddadi et al. using the same setup, indicating that this model still needs refinement to completely encapsulate the inner workings of waterflux in larger tissue.

4.2 Limitations and potential extensions

During the modelling, certain assumptions were made to make the model more abstract. Firstly, one of the simplified compartments is the apoplast space, which is defined as a space where water flows freely, shared by all the cells, where the cell osmotic potential and the apoplasmic water potential are constant over the whole apoplast. This assumption is too strong compared to nature, where the apoplast is very different: it is very much dependent on the position of the cell within the tissue [31]. The osmotic potential is also not defined as a constant, but is different over the whole tissue of the plant [32]. These factors make the assumption that every cell has access to the same apoplast very general, as in the biological case, every cell has access to a different apoplast, which may even be dependent on the topology of the

cell [31]. A potential extension to the model could be the explicit modelling of the apoplast and the topology of a tissue, for example, by extending it into the third dimension. The virtualleaf model is exclusively built in the two-dimensional space, where it is able to simulate flat tissue. However, most plant tissue and organs operate in the three-dimensional space. Expanding virtualleaf into a three-dimensional modelling environment could open the door to simulating whole plant architectures and biomechanical interaction between layers inside the tissue. This would involve the incorporation of three-dimensional meshes instead of two-dimensional polygonal cells, extending the growth rules into three-dimensional space, the wall division procedure and the diffusion of chemicals across the new three-dimensional gradients. Moreover, this would also allow the virtualleaf data to not only be used on two-dimensional microscopy, as shown by Grosseholz et al. [33], but also on three-dimensional microscopy like confocal scanning, allowing more precise comparison between the model and nature. An alluring first step would be to model forces at the bottom and top of the tissue, exploring the effect of a curve on a flat tissue, which could represent many biological cases, such as ferns [34] [35]. However, the expansion into the third dimension comes with an even larger computational cost, as computational power is already a big challenge in modelling.
Lastly, a crucial assumption made by both models is the trigger for cells to divide. In the models, the area of the cell is chosen as a trigger for the cell to divide. However, the division trigger of plant cells is regulated by a complex interplay of positional cues and signals within the tissue. For example, research by Willis et al. [5] showed that cells in the shoot apical meristem of the *Arabidopsis* do not go into the dividing phase at a set size. Instead, research by D'Ario et al. [36] showed that cells gauge their size by the DNA content in the cell by the *KRP4* protein, which binds to the DNA. Like this, cells can measure their size and react to environmental and developmental signals [36]. This makes the cell division process very challenging to model, but these papers could serve as a starting point for a new cell division procedure.
A potential future research in the model could be the simulation of more timesteps for the waterflux models. In this study, the simulation had a maximum of 12000 timesteps. When simulating further, the computing time ramps up massively, and the simulation crashed, making the calculations too difficult for the model. It should be noted that this was done in the ALICE environment of Leiden University, illustrating the computational power the waterflux model requires. This could be optimised in future studies as well, in the form of the model or virtualleaf itself.
In Section 1, an overview was given of the state of research for the division rules. The most recent discovery of the confirmation of the stress-based division, where the cell divides based on the stress, is one of the most accurate division rules yet [18]. Stress has not yet been implemented in virtualleaf and can potentially explain the division of cells in a more realistic way. A thesis by Kok [37] implemented stress-based division in virtualleaf, where it was shown that the cell walls in virtualleaf behave differently than in the model by Louveaux et al. [38], who discovered this rule. The thesis proposed different cell wall yielding mechanics to properly assign the right division axis, but this method is not compatible with the newest version of virtualleaf [37]. We also introduced the Lewis' law, but there is research ongoing for more laws as well. A different formulation was described by Aboav and Weaire on another observation made by Lewis, 'cells with less-edged have a tendency to be in contact with many-edged cells'. Crystallographers refined this theory into the formally known 'Aboav-Weaire law' (AW-law) [39]. The Weaire form of this law is written as the average number of neighbours of the n-sided cell's neighbours m_n as $m_n = (6 - a) + \frac{6a+\mu_2}{n}$, where μ_2 is defined as the variance of the

neighbour distribution over the whole tissue and a is a constant that controls this relation, which is typically defined as $a = 1.2$, as it holds in different biological tissue. However, this formula has shown deviations and errors in cells with 5 to 8 sides and in different structures, a can change considerably and has to be estimated for every tissue [15]. A possible mechanical explanation has been proposed for this law, where Vetter et al. propose that the AW-law emerges from the minimisation of the lateral contact surface energy: when a cell has many neighbours, it tries to reduce the number of neighbours by assuming a more regular shape, closing down on the angle in the junction with other cells, giving way to cells with more neighbours, as the angles at junctions have to always sum to the 360 degress, implying the AW-law to hold [40]. However, this study has yet to be peer-reviewed but may offer an insight on the workings of this law. This law should also be a very interesting law to study in the future.
Finally, it should be noted that the simulation in Section 14 shows an abnormality, mainly for the simulations for the CC- and the ALPHA+ set. Potential issues have been discussed in the previous section, but the balance between the apoplast flux and symplasmic flux is a consideration. In the simulations, the apoplast flux was divided by 100000 to keep the cells in balance while growing. However, this has some further-reaching implications, as this makes the impact of this part of the Hamiltonian less present. Importantly, the equations controlling the water intake have been built with another form of turgor pressure in mind [3] [20], so more research should be conducted to generalise this turgor pressure in the virtualleaf model, by giving it a unit of measurement. Another less discussed point is the choice of the osmotic pressure, which is also an experimentally assessed value which could be more precisely determined.

5 Conclusion

In this paper, the effect of the pressure on the topology and the division methods is studied on plant tissue generated by virtualleaf, with and without the extension of the waterflux-based growth in the cells. The simulation in virtualleaf has shown that the data is too widely spread to make concrete conclusions about most of the relations between the pressure and topological properties of the tissue. However, the relations between the area and the pressure can be partly explained by a negative correlation, which is an interesting discrepancy from the other data. The waterflux model introduced showed that the waterflux behaviour as shown by Cheddadi et al. [3] can be replicated in virtuallea and that the model can even show the flux-lateral inhibition on a multicellular level. However, these simulations showed a lot of discrepancies. Finally, the topology of the waterflux model was studied and showed no significant relations, despite an earlier model built by Long et al. [20] showing negative and positive correlations between topology and pressure. This thesis serves as a starting point into the study of the topology of virtualleaf, as there are many assumptions which may be relaxed to create a more realistic, close to nature resembling tissue, as the development of virtualleaf itself still continues.

6 Supplementary information

6.1 Code

All the code used can be found on https://github.com/wvenemans/master-thesis.
The repository for virtualleaf, including the newest version, can be found at
https://github.com/rmerks/virtualleaf2021 [12].

6.2 Supplemental figures and videos.

6.2.1 Videos

All the videos are online to watch with the vimeo links. Alternatively, all the videos can also be found in the Github repository mentioned in Section 6.1.

- **Video 1**: An example of a tissue growing in virtualleaf using the Errera division procedure, until the 4000 timesteps is reached. Available at: https://vimeo.com/1111933858
- **Video 2** An example of a tissue growing in virtualleaf using the random axis division procedure, until the 4000 timesteps is reached. Available at: https://vimeo.com/1111933904
- **Video 3** A balanced growth between two cells in the two cell model. Available at: https://vimeo.com/1111934041
- **Video 4** An unbalanced growth between two cells in the two cell model. Available at: https://vimeo.com/1111934068
- **Video 5** An example of a tissue growing in virtualleaf using the Errera division porcedure with the waterflux expansion, until the 4000 timesteps is reached. Available at: https://vimeo.com/1111933927
- **Video 6** An example of a tissue growing in virtualleaf using the Random axis division procedure with the waterflux expansion, until the 4000 timesteps is reached. Available at: https://vimeo.com/1111933982

6.2.2 Tables

Simulation	Cell Number	Average Area	Standard Deviation	Average circumference	Standard Deviation	Average pressure	Standard deviation
High α^s, low α^a	Cell 0	993.11	0.77	107.26	1.94	13.79	1.55
	Cell 1	669.97	87.35	87.04	3.20	17.76	2.26
High α^s, balanced α^a	Cell 0	999.21	0.68	115.76	2.13	1.59	1.36
	Cell 1	999.44	0.43	113.13	1.85	1.12	0.86
High α^s, high α^a	Cell 0	999.83	0.70	129.04	3.24	0.33	1.39
	Cell 1	999.51	0.74	125.94	4.39	0.98	1.49
Balanced α^s, low α^a	Cell 0	992.72	0.88	107.08	2.33	14.55	1.77
	Cell 1	703.81	123.17	89.08	6.40	17.66	2.48
Balanced α^s, balanced α^a	Cell 0	999.23	0.56	114.17	1.95	1.53	1.12
	Cell 1	999.22	0.66	113.24	2.28	1.55	1.31
Balanced α^s, high α^a	Cell 0	999.94	0.66	127.83	3.26	0.12	1.31
	Cell 1	1000.03	0.54	125.12	3.89	-0.06	1.09
Low α^s, low α^a	Cell 0	399.49	103.77	88.01	8.34	99.24	7.23
	Cell 1	31.12	31.16	35.81	9.66	151.91	23.14
Low α^s, balanced α^a	Cell 0	999.46	0.65	114.66	1.77	1.08	1.30
	Cell 1	999.19	0.65	113.28	2.26	1.61	1.31
Low α^s, high α^a	Cell 0	999.20	0.70	126.16	4.09	1.60	1.40
	Cell 1	999.52	0.67	118.93	1.89	0.95	1.35

Table 10: The area, circumference of the 9 cells that are shown in Figure 11. Cell 0 is the rightmost cell and cell 1 the leftmost cell in the figures.

References

[1] J. A. Lockhart, "An analysis of irreversible plant cell elongation," *Journal of theoretical biology*, vol. 8, no. 2, pp. 264–275, 1965.

[2] O. Ali, I. Cheddadi, B. Landrein, and Y. Long, "Revisiting the relationship between turgor pressure and plant cell growth," *New Phytologist*, vol. 238, p. 62–69, Jan. 2023.

[3] I. Cheddadi, M. Génard, N. Bertin, and C. Godin, "Coupling water fluxes with cell wall mechanics in a multicellular model of plant development," *PLOS Computational Biology*, vol. 15, p. e1007121, June 2019.

[4] I. Conlon and M. Raff, "Size control in animal development," *Cell*, vol. 96, p. 235–244, Jan. 1999.

[5] L. Willis, Y. Refahi, R. Wightman, B. Landrein, J. Teles, K. C. Huang, E. M. Meyerowitz, and H. Jönsson, "Cell size and growth regulation in the arabidopsis thaliana apical stem cell niche," *Proceedings of the National Academy of Sciences*, vol. 113, Dec. 2016.

[6] H. Czesnick and M. Lenhard, "Size control in plants—lessons from leaves and flowers," *Cold Spring Harbor Perspectives in Biology*, vol. 7, p. a019190, Aug. 2015.

[7] J. K. Ortega, "Augmented growth equation for cell wall expansion," *Plant physiology*, vol. 79, no. 1, pp. 318–320, 1985.

[8] R. Farhadifar, J.-C. Röper, B. Aigouy, S. Eaton, and F. Jülicher, "The Influence of Cell Mechanics, Cell-Cell Interactions, and Proliferation on Epithelial Packing," *Current Biology*, vol. 17, pp. 2095–2104, Dec. 2007.

[9] M. C. Gibson, A. B. Patel, R. Nagpal, and N. Perrimon, "The emergence of geometric order in proliferating metazoan epithelia," *Nature*, vol. 442, pp. 1038–1041, Aug. 2006.

[10] O. Hamant, M. G. Heisler, H. Jönsson, P. Krupinski, M. Uyttewaal, P. Bokov, F. Corson, P. Sahlin, A. Boudaoud, E. M. Meyerowitz, Y. Couder, and J. Traas, "Developmental Patterning by Mechanical Signals in Arabidopsis," *Science*, vol. 322, pp. 1650–1655, Dec. 2008.

[11] K. Alim, O. Hamant, and A. Boudaoud, "Regulatory Role of Cell Division Rules on Tissue Growth Heterogeneity," *Frontiers in Plant Science*, vol. 3, Aug. 2012.

[12] R. M. Merks, M. Guravage, D. Inzé, and G. T. Beemster, "VirtualLeaf: An Open-Source Framework for Cell-Based Modeling of Plant Tissue Growth and Development," *Plant Physiology*, vol. 155, pp. 656–666, Feb. 2011.

[13] G. W. Bassel, P. Stamm, G. Mosca, P. B. de Reuille, D. J. Gibbs, R. Winter, A. Janka, M. J. Holdsworth, and R. S. Smith, "Mechanical constraints imposed by 3d cellular geometry and arrangement modulate growth patterns in the arabidopsis embryo," *Proceedings of the National Academy of Sciences*, vol. 111, no. 23, pp. 8685–8690, 2014.

[14] F. T. Lewis, "The correlation between cell division and the shapes and sizes of prismatic cells in the epidermis of cucumis," *The Anatomical Record*, vol. 38, no. 3, pp. 341–376, 1928.

[15] S. Chiu, "Aboav-weaire's and lewis' laws—a review," *Materials Characterization*, vol. 34, no. 2, pp. 149–165, 1995.

[16] M. Kokic, A. Iannini, G. Villa-Fombuena, F. Casares, and D. Iber, "Minimisation of surface energy drives apical epithelial organisation and gives rise to Lewis' law." BioRxiv [preprint]. 2019 BioRxiv 590729 [posted Mar 2019; cited Aug 2025] Avalaible from: https://www.biorxiv.org/content/10.1101/590729v1.article-info.

[17] L. G. Smith, "Plant cell division: Building walls in the right places," *Nature Reviews Molecular Cell Biology*, vol. 2, pp. 33–39, Jan. 2001.

[18] M. Höfler, X. Liu, T. Greb, and K. Alim, "Mechanical forces instruct division plane orientation of cambium stem cells during radial growth in Arabidopsis thaliana," *Current Biology*, vol. 34, Nov. 2024.

[19] S. Besson and J. Dumais, "Universal rule for the symmetric division of plant cells," *Proceedings of the National Academy of Sciences*, vol. 108, pp. 6294–6299, Apr. 2011.

[20] Y. Long, I. Cheddadi, G. Mosca, V. Mirabet, M. Dumond, A. Kiss, J. Traas, C. Godin, and A. Boudaoud, "Cellular Heterogeneity in Pressure and Growth Emerges from Tissue Topology and Geometry," *Current Biology*, vol. 30, pp. 1504–1516.e8, Apr. 2020.

[21] H. B. Wolff, L. A. Davidson, and R. M. H. Merks, "Adapting a Plant Tissue Model to Animal Development: Introducing Cell Sliding into VirtualLeaf," *Bulletin of Mathematical Biology*, vol. 81, pp. 3322–3341, Aug. 2019.

[22] C. Maurel, Y. Boursiac, D.-T. Luu, V. Santoni, Z. Shahzad, and L. Verdoucq, "Aquaporins in plants," *Physiological reviews*, vol. 95, no. 4, pp. 1321–1358, 2015.

[23] C.-C. Antonovici, G. Y. Peerdeman, H. B. Wolff, and R. M. H. Merks, "Modeling Plant Tissue Development Using VirtualLeaf," in *Plant Systems Biology: Methods and Protocols* (M. Lucas, ed.), pp. 165–198, New York, NY: Springer, 2022.

[24] A. F. M. Marée, V. A. Grieneisen, and P. Hogeweg, "The Cellular Potts Model and Biophysical Properties of Cells, Tissues and Morphogenesis," in *Single-Cell-Based Models in Biology and Medicine* (A. R. A. Anderson, M. A. J. Chaplain, and K. A. Rejniak, eds.), pp. 107–136, Basel: Birkhäuser Basel, 2007.

[25] M. A. de Souza, H. Remigio Gamba, and H. Pedrini, *Multi-Modality Imaging*. Springer, 2018.

[26] R. Merks, R. van Nieuwenhoven, R. Großeholz, and M. Guravage, "Virtualleaf, a cell-based computer modeling framework for simulating plant tissue morphogenesis." https://github.com/rmerks/VirtualLeaf2021/releases/tag/v2.0.0, November 2024.

[27] F. T. Lewis, "A comparison between the mosaic of polygons in a film of artificial emulsion and the pattern of simple epithelium in surface view (cucumber epidermis and human amnion)," *The Anatomical Record*, vol. 50, p. 235–265, Sept. 1931.

[28] F. Pedregosa, G. Varoquaux, A. Gramfort, V. Michel, B. Thirion, O. Grisel, M. Blondel, P. Prettenhofer, R. Weiss, V. Dubourg, J. Vanderplas, A. Passos, D. Cournapeau, M. Brucher, M. Perrot, and E. Duchesnay, "Scikit-learn: Machine learning in Python," *Journal of Machine Learning Research*, vol. 12, pp. 2825–2830, 2011.

[29] D. Kierzkowski, N. Nakayama, A.-L. Routier-Kierzkowska, A. Weber, E. Bayer, M. Schorderet, D. Reinhardt, C. Kuhlemeier, and R. S. Smith, "Elastic domains regulate growth and organogenesis in the plant shoot apical meristem," *Science*, vol. 335, p. 1096–1099, Mar. 2012.

[30] W. T. Gibson, J. H. Veldhuis, B. Rubinstein, H. N. Cartwright, N. Perrimon, G. W. Brodland, R. Nagpal, and M. C. Gibson, "Control of the Mitotic Cleavage Plane by Local Epithelial Topology," *Cell*, vol. 144, pp. 427–438, Feb. 2011.

[31] T. N. Buckley, "The contributions of apoplastic, symplastic and gas phase pathways for water transport outside the bundle sheath in leaves," *Plant, Cell amp; Environment*, vol. 38, p. 7–22, June 2014.

[32] C. Scoffoni, C. Albuquerque, C. R. Brodersen, S. V. Townes, G. P. John, M. K. Bartlett, T. N. Buckley, A. J. McElrone, and L. Sack, "Outside-xylem vulnerability, not xylem embolism, controls leaf hydraulic decline during dehydration," *Plant Physiology*, vol. 173, p. 1197–1210, Jan. 2017.

[33] R. Großeholz, R. W. van Nieuwenhoven, B. H. Mele, and R. M. H. Merks, "Enhanced Cell Wall Mechanics in VirtualLeaf Enable Realistic Simulations of Plant Tissue Dynamics," Aug. 2024.

[34] J. A. Banks, L. Hickok, and M. A. Webb, "The programming of sexual phenotype in the homosporous fern ceratopteris richardii," *International Journal of Plant Sciences*, vol. 154, no. 4, pp. 522–534, 1993.

[35] L. G. Hickok, T. R. Warne, and R. S. Fribourg, "The biology of the fern ceratopteris and its use as a model system," *International Journal of Plant Sciences*, vol. 156, no. 3, pp. 332–345, 1995.

[36] M. D'Ario, R. Tavares, K. Schiessl, B. Desvoyes, C. Gutierrez, M. Howard, and R. Sablowski, "Cell size controlled in plants using dna content as an internal scale," *Science*, vol. 372, p. 1176–1181, June 2021.

[37] A. Kok, "An extension for virtualleaf to explore the mechanical division rule in plant morphogenesis." Thesis, Universisteit Wageningen.

[38] M. Louveaux, J.-D. Julien, V. Mirabet, A. Boudaoud, and O. Hamant, "Cell division plane orientation based on tensile stress in Arabidopsis thaliana," *Proceedings of the National Academy of Sciences*, vol. 113, pp. E4294–E4303, July 2016.

[39] D. Weaire and N. Rivier, "Soap, cells and statistics—random patterns in two dimensions," *Contemporary Physics*, vol. 25, pp. 59–99, Jan. 1984.

[40] R. Vetter, M. Kokic, H. Gómez, L. Hodel, B. Gjeta, A. Iannini, G. Villa-Fombuena, F. Casares, and D. Iber, "Aboave-Weaire's law in epithelia results from an angle constraint in contiguous polygonal lattices," Mar. 2019.